

## THE PERALKALINE TIN-MINERALIZED MADEIRA CRYOLITE ALBITE-RICH GRANITE OF PITINGA, AMAZONIAN CRATON, BRAZIL: PETROGRAPHY, MINERALOGY AND CRYSTALLIZATION PROCESSES

HILTON TULIO COSTI<sup>§</sup>

*Museu Paraense Emílio Goeldi, Laboratório de Microscopia Eletrônica de Varredura and Instituto de Geociências, Universidade Federal do Pará, CP 8608, 66075-100, Belém, PA, Brazil*

ROBERTO DALL'AGNOL

*Instituto de Geociências, Universidade Federal do Pará, CP 8608, 66075-100, Belém, PA, Brazil*

MICHEL PICHAVANT

*Institut des Sciences de la Terre d'Orléans, UMR 6113 CNRS-Université d'Orléans, 1A, rue de la Férollerie, F-45071 Orléans, Cedex 02, France*

OSMO TAPANI RÄMÖ

*Department of Geology, P.O. Box 64, FI-00014 University of Helsinki, Finland*

### ABSTRACT

The 1.818 Ga magmatic, subsolvus, Madeira albite-rich granite of the Pitinga province, exploited at the Pitinga mine, in northern Brazil, crystallized from a F-rich melt, also enriched in Sn, Rb, and HFSE. It is composed of a peralkaline, cryolite-bearing core facies and a peraluminous to metaluminous, oxidized, fluorite-bearing border facies, generated by autometamorphic processes after the crystallization of the core facies. A metaluminous to peralkaline hypersolvus granite is comagmatic with the albite-rich granite. Petrographic studies indicate that quartz was the first phase to crystallize, at ~700°C; the quartz – K-feldspar cotectic was attained at around 650°C, and the ternary feldspar solvus and onset of albite crystallization down to the solidus, estimated at around 500°C. Massive cryolite and pegmatitic rocks found in the center of the stock were derived from the residual melt. The albite-rich granite probably originated by crystallization of a dense, F-rich, peralkaline phase derived from a peralkaline to metaluminous parental melt by immiscibility.

**Keywords:** albite-rich subsolvus granite, peralkaline, tin, niobium, cryolite, immiscibility, Madeira granite, Pitinga mine, Brazil.

### SOMMAIRE

Le granite subsolvus de Madeira, enrichi en albite d'origine magmatique (1.818 Ga), a cristallisé à partir d'un magma riche en fluor et enrichi en étain, rubidium, et éléments à champ électrostatique élevé; il est exploité à la mine Pitinga, dans le nord du Brésil. Ce granite est hyperalkalin, et contient un faciès à cryolite au centre, et un faciès de bordure hyperalumineux à métalumineux à fluorite, oxydé, et généré par autométasomatose suite à la formation du faciès à cryolite. Un granite hypersolvus métalumineux à hyperalkalin est comagmatique avec le granite enrichi en albite. Nos observations pétrographiques montrent que le quartz a été la première phase à cristalliser, à environ 700°C; la courbe cotectique impliquant le quartz et le feldspath potassique a été atteint à environ 650°C, et le solvus dans le système ternaire Ab–Or–An a été croisé, pour initier la cristallisation de l'albite jusqu'au solidus, à environ 500°C. Des accumulations massives de cryolite et des roches pegmatitiques situées près du centre du pluton sont dérivées de magmas résiduels. Le granite enrichi en albite aurait cristallisé aux dépens d'une venue dense, riche en fluor et hyperalkaline, dérivée à partir d'un magma parent hyperalkalin à métalumineux par immiscibilité.

(Traduit par la Rédaction)

**Mots-clés:** granite subsolvus riche en albite, hyperalkalin, étain, niobium, cryolite, immiscibilité, granite de Madeira, mine de Pitinga, Brésil.

<sup>§</sup> E-mail address: [artur.bastos@ufrgs.br](mailto:artur.bastos@ufrgs.br)



## INTRODUCTION

Evolved granitic plutons such as leucogranites and albite granites are an important source of Sn, W, Nb, Ta, U, Zr and Th (Pichavant & Manning 1984). The origin of albite-enriched granites remains a matter of considerable controversy. The hypothesis of a magmatic origin (Kovalenko & Kovalenko 1984, Pichavant *et al.* 1987, Cuney *et al.* 1992, Xiong *et al.* 1999) has been gradually put forward as an alternative to the traditional idea of a metasomatic origin (Beus 1982, Horbe *et al.* 1991). A closely related issue concerns the effect of F on the crystallization of leucogranitic magmas. This topic has been studied experimentally by Wyllie & Tuttle (1961), Glyuk & Anfilogov (1973), Kovalenko (1978), Manning (1981), Pichavant & Manning (1984), Dingwell (1988), Dingwell *et al.* (1998), Xiong *et al.* (1999, 2002), Dolejs & Baker (2004, 2007a, b, Lukkari & Holtz 2007), among others. From the geochemical point of view, albite-enriched granites are most commonly peraluminous and more rarely peralkaline (Harris 1981, Ekwere & Olade 1984, Bowden & Kinnaird 1984). However, studies of melt inclusions have recently shown that peralkaline melt fractions may be generated during differentiation of peraluminous magmas (Thomas *et al.* 2006). In contrast to peraluminous or metaluminous leucogranites, which probably include a major crustal component, a mantle source has been commonly proposed for peralkaline granites (Baker & McBirney 1985, Nardi & Bonin 1991, Bonin 1996). As an alternative, it has been suggested that peralkaline granitic felsic magmas may have a crustal source [Bailey & Macdonald 1970, Macdonald *et al.* 1987, Scaillet & Macdonald 2003; see Martin (2006) for a review].

The Madeira albite-rich granite of Pitinga, Amazonian craton, Brazil, is a rare example of peralkaline F-rich granite that hosts a major primary deposit of Sn, Nb, Ta, U, Zr and Th. This granite represents one of the few examples of an economic tin deposit associated with an evolved peralkaline granitic magma (Pollard 1995). This paper is focused on the relative importance of magmatic *versus* hydrothermal processes in the petrogenesis of evolved granites and the role of F in crystallization-differentiation. Other relevant related topics, such as the geochemical evolution and origin of evolved peralkaline albite-rich granitic magmas, will be discussed in forthcoming papers. In this paper, we describe the geological setting, petrography, and mineralogy of the Madeira albite-rich granite of the Pitinga province and discuss a crystallization model for this type of peralkaline albite-rich subsolvus granite.

## GEOLOGICAL SETTING

The Pitinga Province, located in the southern part of the Guiana Shield (Gibbs & Barron 1983, Almeida *et al.* 2000), belongs to the Central Amazonian Province

of the Amazonian craton (Tassinari & Macambira 1999, Santos *et al.* 2000). The main geological aspects of the region were reviewed by Costi *et al.* (2000a). Paleoproterozoic calc-alkaline granitic rocks of the Água Branca suite, the A-type or calc-alkaline silicic volcanic rocks of the Iricoumé Group (Uatumã Supergroup) and the associated A-type granites of the Mapuera Suite are dominant in the Province (Fig. 1a). From the end of the Paleoproterozoic until the beginning of the Neoproterozoic, the evolution of the Amazonian craton shows many parallels to the North American and Fennoscandian shields (*e.g.*, Brito Neves & Cordani 1991, Sadowski & Bettencourt 1996). During this time, several magmatic events led to the generation of widespread occurrences of rapakivi granite in the Amazonian craton (Dall'Agnol *et al.* 1999, Bettencourt *et al.* 1999). The rapakivi granite suites intrude the Paleoproterozoic calc-alkaline granitic rocks and the Iricoumé volcanic rocks (Dall'Agnol *et al.* 1999, Costi *et al.* 2000a; Fig. 1a).

The A-type rapakivi granites of the craton are dominantly metaluminous to peraluminous, and their evolved facies are commonly tin-mineralized (Horbe *et al.* 1991, Dall'Agnol *et al.* 1993, 1999, Bettencourt *et al.* 1999, Costi 2000, Costi *et al.* 2000a, Leite Junior 2002, Teixeira *et al.* 2002, Lenharo *et al.* 2002, 2003). The Pitinga province is one of the most important tin provinces of the Amazonian craton and comprises a cogenetic assemblage of metaluminous to peraluminous leucogranites of the rapakivi series. A peculiar peralkaline albite-rich granite, strongly mineralized in cassiterite and cryolite, is also present in the Madeira pluton of the province (Fig. 1b), and is the focus of our investigation.

*Geology of the Pitinga region*

The main geological units of the Pitinga region are the calc-alkaline granitic rocks of the Água Branca Suite and the volcanic rocks of the Iricoumé Group. These are intruded by two suites of A-type granite, Mapuera and Madeira (Ferron *et al.* 2006, Fig. 1a). The Madeira suite comprises the Europa, Madeira, and Água Boa plutons (Horbe *et al.* 1991, Costi *et al.* 2000a, Ferron *et al.* 2006, Fig. 1a). These are overlain by clastic sedimentary rocks and pyroclastic sheets of the Urupi Formation, and by a set of hypabyssal tholeiitic rocks of the Quarenta Ilhas Formation ( $1780 \pm 3$  Ma; Santos *et al.* 2002). Alkali basalts and diabase dikes of the Seringa Formation, dated at  $\sim 1100$  Ma (Veiga *et al.* 1979), are the youngest magmatic rocks identified in this area.

The Iricoumé Group is composed of rhyolite, dacite, andesite, trachyte, quartz trachyte, and pyroclastic rocks, dominantly tuffs and ignimbrites. The felsic volcanic rocks display A-type geochemical signature (Ferron *et al.*, in press), whereas the intermediate rocks have an ambiguous geochemical character.

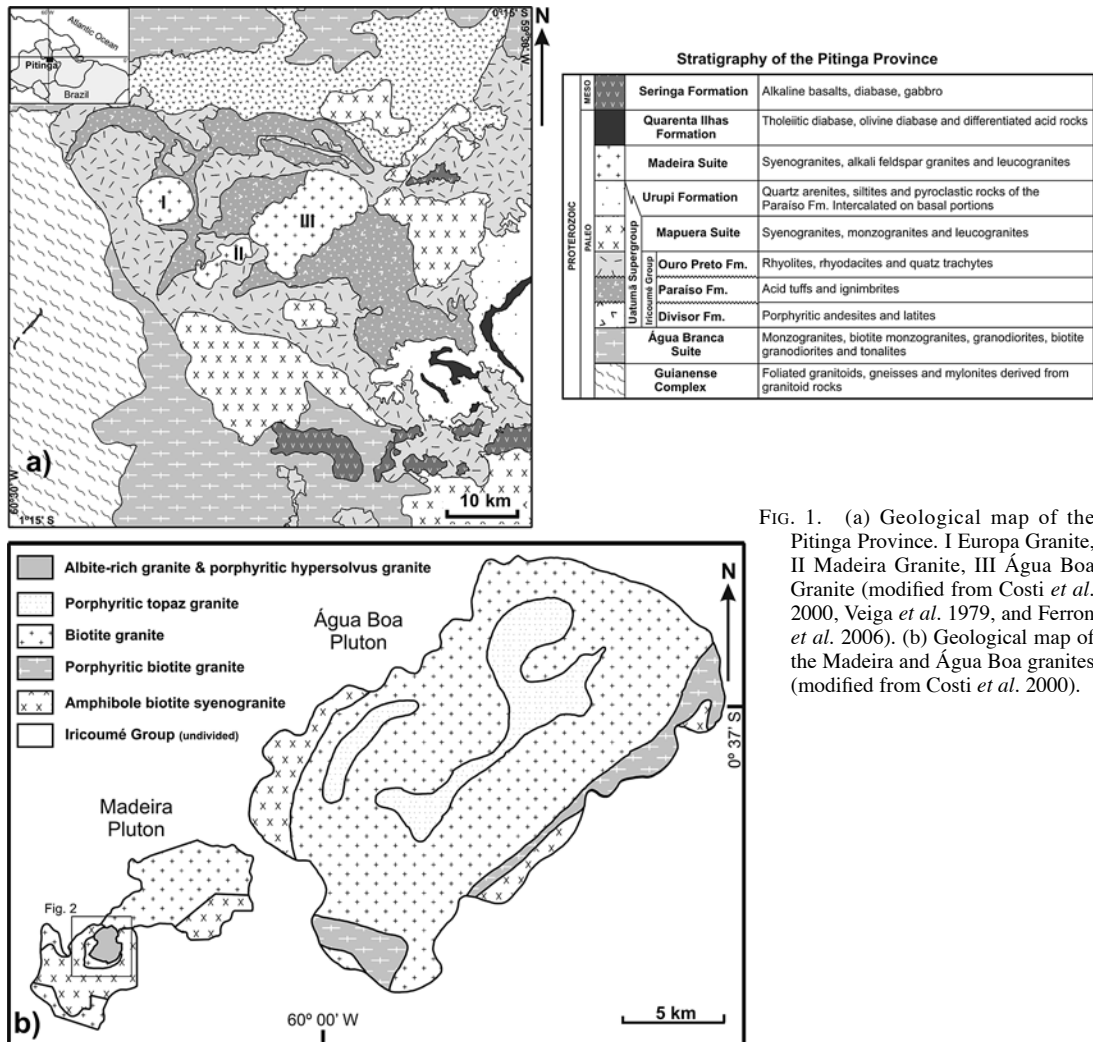


FIG. 1. (a) Geological map of the Pitinga Province. I Europa Granite, II Madeira Granite, III Água Boa Granite (modified from Costi *et al.* 2000, Veiga *et al.* 1979, and Ferron *et al.* 2006). (b) Geological map of the Madeira and Água Boa granites (modified from Costi *et al.* 2000).

Nine samples of this unit yielded  $^{207}\text{Pb}/^{206}\text{Pb}$  zircon-evaporation ages of 1889–1888 Ma (Costi *et al.* 2000a, Ferron *et al.* 2006). The contacts between the Iricoumé Group and the Madeira suite granite plutons are sharp, and centimeter- to meter-size enclaves of the volcanic rocks are found as inclusions in the granites.

#### GEOLOGICAL ASPECTS OF THE GRANITE PLUTONS OF THE MADEIRA SUITE

The Madeira and Água Boa plutons are the main carriers of tin exploited in the Pitinga region. As a result, they have been studied in considerable detail (Macambira *et al.* 1987, Daoud 1988, Horbe *et al.* 1991, Costi 2000, Costi *et al.* 2000a, Lenharo *et al.* 2002, 2003). The early facies of the Água Boa pluton is a coarse-grained

pyterlitic amphibole–biotite syenogranite, known as the rapakivi facies (Fig. 1b). It is followed, successively, by a fine-grained porphyritic biotite syenogranite, a coarse- to medium-grained biotite alkali feldspar granite, and a topaz-bearing porphyritic biotite granite (Daoud 1988, Lenharo *et al.* 2002, 2003). In the Água Boa pluton, primary deposits of tin are associated with greisens (Daoud 1988, Borges *et al.* 2003, 2009) and episyenites (Costi *et al.* 2002).

The Europa granite is a circular pluton composed of a peralkaline, hypersolvus alkali feldspar granite with a  $^{207}\text{Pb}/^{206}\text{Pb}$  zircon-evaporation age of  $1829 \pm 1$  Ma (Costi *et al.* 2000a). Most of the pluton is located in an Indian reservation (Fig. 1a) and, owing to legal issues, is inaccessible to geological work. There is no known tin mineralization related to the Europa granite, however.

The Madeira pluton comprises various facies (Costi 2000, Costi *et al.* 2000a), the less evolved of which being petrographically similar to those in the Água Boa pluton (Horbe *et al.* 1991, Lenharo *et al.* 2002, 2003). The early metaluminous porphyritic amphibole–biotite syenogranite facies commonly shows phenocrysts of plagioclase-mantled alkali feldspar and, locally, fine-grained rounded enclaves of volcanic rocks. This “rapakivi facies” is intruded by a peraluminous to metaluminous, equigranular biotite alkali feldspar granite. Enclaves of the earlier facies are found in the biotite granite along the contacts. Costi *et al.* (2000a) reported

$^{207}\text{Pb}/^{206}\text{Pb}$  zircon-evaporation ages of  $1824 \pm 2$  Ma and  $1822 \pm 2$  Ma for the amphibole–biotite syenogranite and biotite alkali feldspar granite facies, respectively. Both facies are intruded by a near-circular stock with a diameter of  $\sim 2$  km composed of the albite-rich granite and the porphyritic hypersolvus granite (Fig. 1b).

The circular stock has been in part mapped at the 1:500 scale and was the target of an extensive drilling program (Fig. 2a). It is a sheet-like intrusion with an upper layer of subsolvus albite-rich granite and an underlying sheet of porphyritic hypersolvus metaluminous alkali feldspar granite (Fig. 2b). The porphyritic hypersolvus alkali feldspar granite is exposed only in the western part of the stock, where it is in contact with the border facies of the albite-rich granite. Contacts between the albite-rich granite and the biotite alkali feldspar granite are not exposed. Further information comes from drill holes; the porphyritic hypersolvus alkali feldspar granite is in contact with the core facies of the albite-rich granite (*cf.* Fig. 2b). The albite-rich granite is composed of a peralkaline, gray cryolite-bearing core facies (AbGC) and a surrounding peraluminous, deep red, fluorite-bearing border facies (AbGB; Costi 2000, Costi *et al.* 2000a). The transition between the core and border facies is gradational.

In drill core, the AbGC displays sinuous or inter-fingering contacts with the porphyritic hypersolvus alkali feldspar granite. Additional evidence of interaction between both “magmas” is given by the presence in the AbGC of perthitic alkali feldspar xenocrysts derived from the porphyritic hypersolvus alkali feldspar granite (Costi *et al.* 2000a). In some places, the alkali feldspar phenocrysts of the porphyritic hypersolvus alkali feldspar granite are corroded and show cavities filled by cryolite. Near the contact with the albite-rich granite, the hypersolvus granite displays abundant bipyramidal crystals of zircon, similar to those found in the albite-rich granite. Costi *et al.* (2000a) concluded that the hypersolvus granite and the albite-rich granite are coeval. They obtained a  $^{207}\text{Pb}/^{206}\text{Pb}$  zircon-evaporation age of  $1818 \pm 2$  Ma for the porphyritic hypersolvus alkali feldspar granite and assumed a similar age of crystallization for the albite-rich granite.

In the exposed part of the pluton, the porphyritic hypersolvus alkali feldspar granite is in contact only with the AbGB. The contact relationships are similar to those seen in the drill cores. However, along the contact between the AbGB and the porphyritic hypersolvus alkali feldspar granite, the latter is brick red color and intensely oxidized and shows evidence for albitization or episyenitization (or both). These features indicate that hydrothermal processes observed in the AbGB also affected the hypersolvus granite.

A cryolite deposit comprising pods and massive veins  $\sim 0.5$  to 50 m thick intercalated with the AbGC is found  $\sim 100$  m below the present surface of the albite-rich granite sheet (Fig. 2b; Costi *et al.* 2000a). Coarse-grained, meter-thick layers of quartz or perthitic

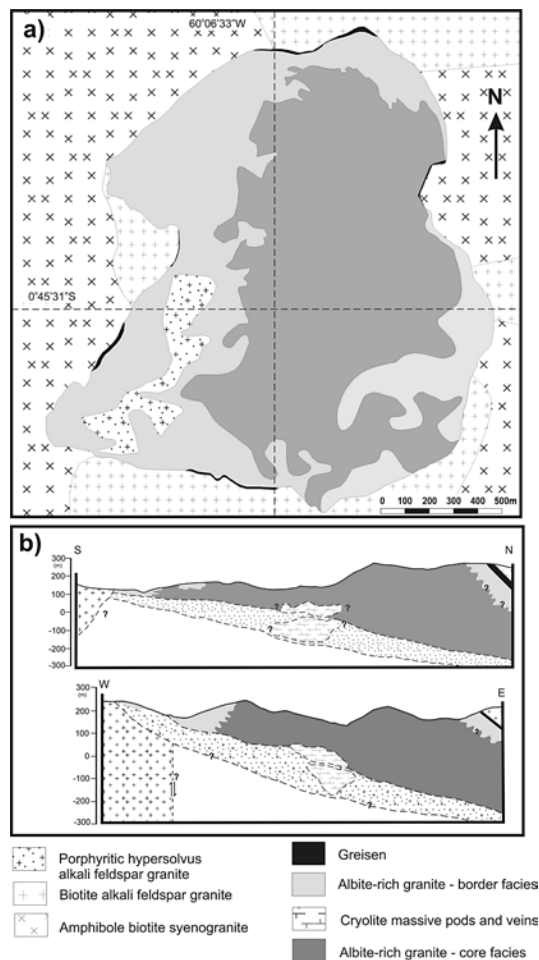


FIG. 2. A). Geological map of the albite-rich granite and porphyritic hypersolvus granite (modified from Minuzzi 2005). B). Schematic profiles along the central part of the albite-rich granite, showing the contacts with the early facies and the position of the cryolite-rich zone at the inner core of the albite-rich granite. The vertical scale is equal to the horizontal scale (modified from Costi *et al.* 2000).

feldspar or massive lithium–iron mica are associated with the cryolite veins, suggesting that processes generally associated with pegmatitic suites were involved in the evolution of the massive cryolite and associated rocks (Costi 2000, Minuzzi 2005, Minuzzi *et al.* 2008, Bastos Neto *et al.* 2005).

The core facies of the albite-rich granite includes “quartz syenitic”, albite-rich rocks with a fluidal texture. They show transitional contacts with the albite-rich granite and, locally, with pegmatitic pods ~50 cm in diameter.

#### ANALYTICAL TECHNIQUES

##### *Petrography*

Our petrographic studies involved a macroscopic examination and logging of *ca.* twenty thousand meters of drill holes in the albite-rich granite stock and nearby country rocks. About 2500 thin sections of selected samples were available for petrographic studies. Samples of twenty drill-holes were studied in detail, involving classical petrographic optical microscopy and textural analysis for definition of the crystallization sequence of minerals in the albite-rich granite. Opaque minerals, iron–titanium oxides in particular, were studied in a preliminary way by reflected light microscopy techniques (Almeida 2002).

Modal analyses were done with a Swift automatic point counting coupled to an optical microscope (~3500 points were counted for each thin section). Only one counting was done for each section, but this was compensated by the fact that several samples of each variety of albite-rich granites have been analyzed.

##### *Scanning electron microscopy (SEM)*

Textural relationships among the various minerals (exsolution, inclusion, zoning and replacement textures) were studied by back-scattered SEM images. Special attention was given to feldspars, micas, alkali amphibole, zircon, cassiterite, magnetite, and pyrochlore. Qualitative chemical analyses of these minerals were made employing the EDS technique.

##### *Electron-microprobe and ion-microprobe analyses*

Most minerals were analyzed at the University of Brasília (UnB) using a Cameca SX50 electron microprobe using a 15 kV acceleration voltage, 25 nA sample current, and 10 s total of counting time. Silicate minerals and synthetic glasses were used as standards, and the data were corrected with the PAP correction program. Additional analyses of micas were done at the Bureau des Recherches Géologiques et Minières (BRGM) at Orléans, France, using a Camebax electron microprobe under similar analytical conditions.

The Rb, Cs, and Be contents of micas were established using a Cameca IMS3F ion microprobe at the Centre des Recherches Pétrographiques et Géochimiques, Vandoeuvre-lès-Nancy, France.

#### PETROGRAPHY OF THE MADEIRA PLUTON

##### *Amphibole–biotite syenogranite*

The amphibole–biotite syenogranite is porphyritic or seriate and consists of perthitic alkali feldspar (60–75%), quartz (20–30%), and plagioclase (<10%) with subordinate biotite and hornblende. The phenocrysts are subhedral or oval-shaped, ~5 to 10 mm long alkali feldspar crystals locally mantled by plagioclase. They are set in a fine- to medium-grained, occasionally granophyric groundmass of alkali feldspar, quartz and plagioclase. In some samples, minor amphibole-rimmed clinopyroxene crystals are present. The mafic phases form rounded clots that also contain zircon, apatite, opaque minerals, titanite, and fluorite.

##### *Biotite alkali feldspar granite*

The biotite alkali feldspar granite is a leucocratic, medium- or fine-grained equigranular rock consisting of mesoperthitic alkali feldspar (55–60%), quartz (30–35%), plagioclase (0–10%), and biotite (1–5%), with accessory fluorite, zircon, and topaz (Daoud 1988, Horbe *et al.* 1991). Subhedral crystals of mesoperthitic alkali feldspar, quartz, and tabular plagioclase form a granular texture. The alkali feldspar is partially replaced by chessboard albite and shows swapped rims of albite. The plagioclase is scarce or absent, suggesting that liquid crystallization could initiate in the plagioclase stability field, forming a limited volume of plagioclase. Subsequently, the liquid composition evolved to the alkali feldspar solid-solution field, where only alkali feldspar is formed, and the crystallization ended in hypersolvus conditions (Tuttle & Bowen 1958, p. 133–135). The biotite is found as fine-grained flakes partially replaced by chlorite.

##### *Porphyritic hypersolvus alkali feldspar granite*

The porphyritic hypersolvus alkali feldspar granite shows euhedral, phenocrysts of perthitic alkali feldspar and quartz 3 to 15 mm across and a fine-grained matrix composed of alkali feldspar, quartz and late intergranular albite. The accessories are biotite, fluorite, zircon, and opaque minerals. Some samples show scattered crystals of blue alkali amphibole and pyrochlore. The quartz phenocrysts are euhedral, and some of them show evidence for being rounded or embayed. The porphyritic hypersolvus alkali feldspar granite is affected by albitization along the contacts with the albite-rich granite and, in particular, in the zones close to the massive cryolite zones.

*Albite-rich granite*

The core (AbGC) and the border (AbGB) facies of the albite-rich granite have generally similar petrographic aspects (Horbe *et al.* 1991), but show, however, clear differences in texture and modal composition (Costi 2000; Table 1). The main compositional feature of the AbGC is the remarkably constant proportions of K-feldspar, albite and quartz (Table 1, Fig. 3a). Compared to the AbGC, the AbGB facies shows generally higher quartz and lower albite, but K-feldspar proportions are similar (Table 1). Therefore, except for some quartz syenitic, albite-rich samples with a fluidal texture, the AbGC samples cluster near the center of

the Qtz–Ab–Or diagram, whereas the AbGB samples are more scattered (Fig. 3a). Modal composition data point to several first-order differences between the two facies: (1) micas are present in the core but are absent in the border facies; (2) cryolite is systematically present in the core facies (it is the most abundant phase after quartz and feldspars, with an average modal content of ~6%, Table 1), whereas the main F-bearing phase in the border facies is fluorite; (3) pyrochlore is only found in the core facies; (4) magnetite is the dominant iron oxide mineral in the core, whereas in the border facies, hematite is a prominent phase. Both facies have relatively high modal contents of cassiterite and zircon, and both contain thorite. Carbonates, sphalerite (core

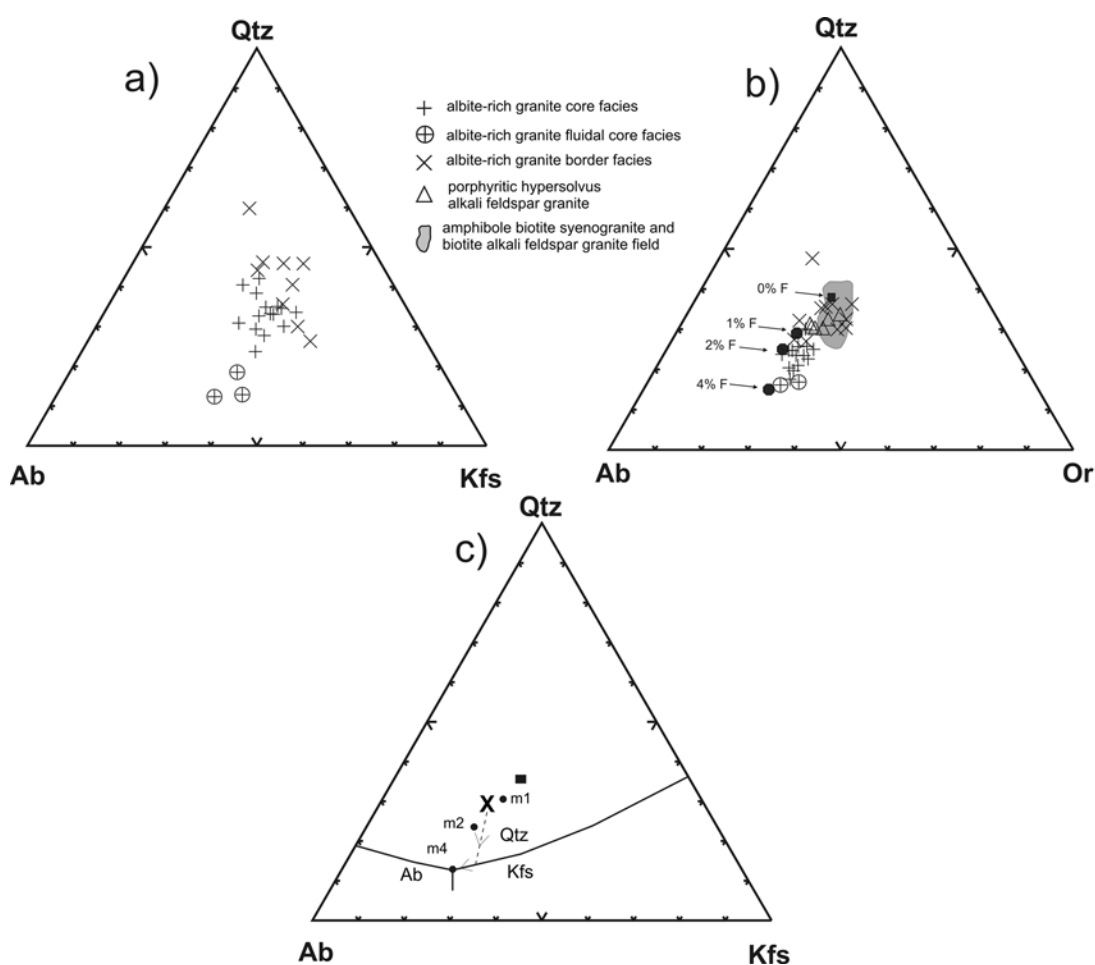


FIG. 3. Modal (a) and CIPW-normative (b) compositions of the albite-rich granite facies of the Madeira pluton. Also plotted in b) are the F-free minimum of Tuttle & Bowen (1958), shown by a filled square, the minima (m) for 1%, 2% and 4% F of Manning (1981) for a H<sub>2</sub>O pressure of 100 MPa, shown by filled circles, and the field of the amphibole–biotite syenogranite and biotite alkali feldspar granite facies of the Madeira pluton. c) Suggested path of crystallization for the albite-rich granite. X marks the inferred initial composition of the albite-rich granite melt.

TABLE 1. MODAL COMPOSITION OF THE ALBITE-RICH GRANITE FACIES OF THE MADEIRA GRANITE

Sample	Ab	Kfs	Qtz	LiAnn	Chl	Pln	Cry	Fl	Zrn	Pcl	Opq	Thr	Rbk	Cst
<b>Albite-rich granite, core facies</b>														
82a	26.0	36.5	26.9	-	-	1.8	5.6	-	0.9	0.4	0.3	-	1.5	0.1
83	23.8	24.6	35.2	0.2	-	6.3	6.9	-	1.4	0.4	0.8	-	0.2	0.1
120a	22.9	28.5	25.5	1.2	-	2.7	9.5	-	2.1	0.6	0.1	-	6.7	0.2
127.1 <sup>1*</sup>	46.2	30.3	10.7	6.0	-	1.8	2.2	-	0.6	0.8	0.2	0.1	0.3	0.2
127.2 <sup>*</sup>	39.0	31.6	16.0	4.4	-	2.1	3.4	-	0.7	0.7	0.3	-	1.3	0.1
130 <sup>2</sup>	32.4	32.2	20.3	0.6	-	3.1	6.7	-	0.6	0.8	0.3	0.2	1.7	-
135 <sup>3</sup>	28.0	31.6	31.9	0.5	-	1.7	3.8	-	0.5	0.3	0.3	0.1	0.7	tr.
136 <sup>*</sup>	43.4	37.6	12.0	2.4	-	1.6	1.9	-	0.3	0.6	0.1	0.1	tr.	0.1
137	31.1	24.8	25.0	3.4	-	3.0	7.1	-	2.6	0.4	0.2	-	2.4	-
138 <sup>4</sup>	26.8	21.9	33.2	4.5	-	2.9	6.8	-	1.8	0.2	tr.	-	1.8	tr.
142	27.3	32.5	29.7	0.1	-	2.0	5.4	-	0.3	0.8	0.2	-	1.8	-
142a <sup>5</sup>	31.8	31.4	26.1	1.5	-	2.2	4.5	-	0.4	0.3	0.4	0.2	0.8	0.1
143	28.3	28.1	35.1	0.6	-	1.6	5.4	-	0.3	0.2	0.2	-	0.4	-
158	29.6	32.3	23.7	tr.	-	1.4	7.3	-	2.1	0.5	1.8	0.3	0.7	0.2
159	31.5	34.1	25.9	0.2	-	1.3	4.4	-	1.1	0.4	0.5	-	0.5	-
160 <sup>6</sup>	20.2	34.2	27.6	0.6	-	4.7	4.3	-	1.2	1.1	0.1	-	5.5	0.3
161 <sup>7</sup>	29.4	28.9	18.1	0.2	-	2.4	14.8	-	1.7	0.7	2.6	-	1.0	-
162	24.9	34.6	31.4	2.1	-	1.8	3.4	-	0.3	0.5	0.3	-	0.6	0.1
163 <sup>8</sup>	30.5	31.4	30.0	1.1	-	0.8	3.4	-	0.5	0.2	0.7	-	1.0	0.1
165	24.2	32.0	30.3	2.4	-	1.0	7.8	-	1.5	0.6	0.2	-	tr.	-
Mean	29.8	31.0	25.7	1.8	-	2.3	5.7	-	1.1	0.5	0.5	0.2	1.5	0.1
<b>Albite-rich granite, border facies</b>														
93a <sup>9</sup>	18.7	28.9	40.4	-	6.7	-	-	2.1	2.2	-	0.6	0.2	-	0.2
134 <sup>10</sup>	40.7	34.3	19.9	-	0.5	-	-	tr.	0.8	-	1.8	0.1	-	0.4
139	24.0	34.3	32.3	-	4.6	-	-	1.5	3.3	-	0.2	-	-	-
139a	26.6	25.9	40.6	-	1.9	-	-	2.4	2.2	-	0.1	0.1	-	0.2
140	24.6	27.2	44.5	-	0.1	-	-	0.3	2.5	-	0.8	-	-	-
141 <sup>11</sup>	16.0	13.6	43.9	-	-	tr.	-	9.9	0.3	-	0.7	-	-	-
146 <sup>12</sup>	21.7	36.5	25.0	-	-	tr.	-	3.6	3.8	-	6.6	-	-	-
147 <sup>13</sup>	15.9	34.9	43.0	-	-	-	-	0.6	1.2	-	2.6	-	-	0.1
150	24.8	47.7	25.9	-	0.6	-	-	0.2	0.2	-	0.5	-	-	-
151 <sup>14</sup>	21.1	36.1	39.0	-	1.6	-	-	0.1	0.8	-	0.7	-	-	0.4
Mean	23.4	31.9	35.4	-	2.3	-	-	2.3	1.7	-	1.4	0.1	-	0.2

Mineral symbols after Kretz (1983) and Spear (1993); in addition, LiAnn: lithian annite, and Opq: opaque minerals; tr.: traces. \* Fluidal albite-rich quartz syenitic rock. 1) sphalerite 0.25%, carbonate 0.42%; 2) iron hydroxide 0.84%; 3) K-feldspar of adularia habit 0.26%, iron hydroxide 0.23%, aegirine 0.03%, carbonate 0.03%; 4) unidentified mineral (alteration of cryolite) 0.17%; 5) aegirine 0.25%; 6) aegirine 0.14%; 7) unidentified mineral (alteration of cryolite) 0.26%; 8) chlorite 0.35%; 9) sphalerite 0.11%; 10) phengite 1.7%; 11) phengite 15.6%; 12) phengite 2.7%, hematite 0.19%; 13) phengite 0.9%, sphalerite 0.04%; 14) sphalerite 0.19%.

facies), xenotime, galena, pyrite (border facies), and other rare minerals (catapleite, genthelvite, bastnäsité, prosopite) have also been observed.

The AbGC, a grayish rock, shows a medium- to fine-grained seriate or, locally, porphyritic texture. It is characterized by an assemblage of peralkaline minerals. In addition to quartz, K-feldspar, and albite, Fe-Li mica, polyolithionite, cassiterite, magnetite, zircon, cryolite, riebeckite, pyrochlore, plus minor amounts of aegirine and catapleite are present in the core facies (Table 1). Textural observations indicate that quartz was the first phase to crystallize (Fig. 4). Quartz grains are subhedral to euhedral, generally 1 to 5 mm in diameter. Inclusions of albite laths (snowball texture, Beus 1982, Schwartz 1992, Yin *et al.* 1995, Helba *et al.* 1997), concentrated preferentially along the marginal portions of quartz

crystals, are common (Figs. 5a, b). K-feldspar (1 to 2 mm) is subhedral and optically homogeneous, only rarely showing very thin perthitic films. It was the second phase to crystallize. Albite is found as individual twinned clear, subhedral laths that are smaller than the K-feldspar grains. The lack of swapped rims and of late intergranular albite along the contacts of K-feldspar grains is remarkable, indicating no significant processes of late albitization. The Fe-Li mica is pleochroic in shades of brown and green, subhedral (Figs. 5e, f) and commonly includes albite laths. It is locally replaced by cryolite or riebeckite or, in the albite-rich quartz syenitic rocks, by stilpnomelane (Figs. 5g, h). It was the first mafic mineral in the crystallization sequence. Polyolithionite shows moderately pleochroic, colorless to pale blue, ~0.5 to 2.5 mm long crystals (Figs. 5c, d).

Colorless border zones are observed in some cases. Polythionite is unaltered, displays regular contacts with the Li-Fe mica, shows inclusions of albite and probably began to precipitate almost simultaneously with the Fe-Li mica (Figs. 6a, b). It is commonly associated with cryolite and remained in equilibrium with the residual melt until the final stages of crystallization. *Zircon* (Figs. 5e, f) is found as exceptionally large (>3 to 0.5 mm), euhedral, bipyramidal crystals with inclusions of albite, K-feldspar, cryolite, thorite, and magnetite. It is commonly corroded (Figs. 6c, d), with a large sieve-textured metamict core containing significant amounts of H<sub>2</sub>O (A.M. Horbe, pers. commun.), surrounded by thin, clean, Hf-enriched border zones. *Cassiterite* is found as subhedral, dark red to yellowish red, moderately to strongly pleochroic, irregularly zoned crystals with a grain size ranging between 3 and 0.1 mm (Figs. 5c, d). It is disseminated throughout the rock and commonly forms short, twinned prisms with straight contacts with quartz, albite, and K-feldspar. *Magnetite* is either present as fine-grained (up to 0.5 mm), subhedral or euhedral individual crystals, or it forms aggregates associated with riebeckite, Fe-Li mica, cassiterite, or zircon. Magnetite inclusions are found in micas and riebeckite. In some samples, magnetite has been replaced by secondary hematite (Almeida 2002). Zircon, cassiterite and magnetite all crystallized in the same temperature range, and began to precipitate shortly after the beginning of mica crystallization (Fig. 4). Consequently, cassiterite is a magmatic mineral in the albite-rich granite (Costi *et al.* 2000b). *Cryolite* is found as fine-grained, anhedral late-precipitated crystals disseminated among the feldspars (Fig. 5c),

quartz and mafic phases. It also forms coarse-grained aggregates (Fig. 5e) with zircon, cassiterite, micas, and riebeckite. Deep to indigo blue *riebeckite* forms subhedral, prismatic, individual crystals, nest-like aggregates of fibrous crystals, or relatively large (up to 10 mm long) poikilitic crystals. The latter may include albite, quartz, mica, magnetite, cassiterite, and cryolite. Riebeckite, one of the latest magmatic phases, is locally replaced by granular *aegirine*. *Pyrochlore* is a common mineral in the AbGC, occurring as fine-grained (ca. 0.5 mm), euhedral to anhedral, zoned and strongly reddish brown to yellowish brown crystals. It commonly shows a thin reaction border along its contacts with albite and K-feldspar, and is in some places altered to columbite, along fractures and border zones. *Thorite* forms opaque euhedral to subhedral, bipyramidal, fine-grained crystals that are strongly metamict (Fig. 5c). *Catapleiite* occurs only locally in the AbGC, as euhedral, prismatic, fine- to medium-grained poikilitic crystals that include quartz, cryolite, feldspars and micas. *Siderite* and *sphalerite* are secondary minerals found in the fluidal albite-rich quartz syenite.

The AbGB is a reddish, strongly oxidized rock, texturally generally similar to the AbGC. In thin section, it is turbid owing to ubiquitous dust-size grains of iron oxides (Figs. 5i, j). Cavities filled by late quartz, probably formed by dissolution of the primary phases, are commonly observed throughout the AbGB (Figs. 5k, l). These textural aspects, combined with the mineralogical evidence, indicate that autometasomatic processes were important in the generation of the AbGB at the expense of the AbGC (Costi 2000). *Albite* shows evidence of partial dissolution and replacement by quartz. *Zircon*

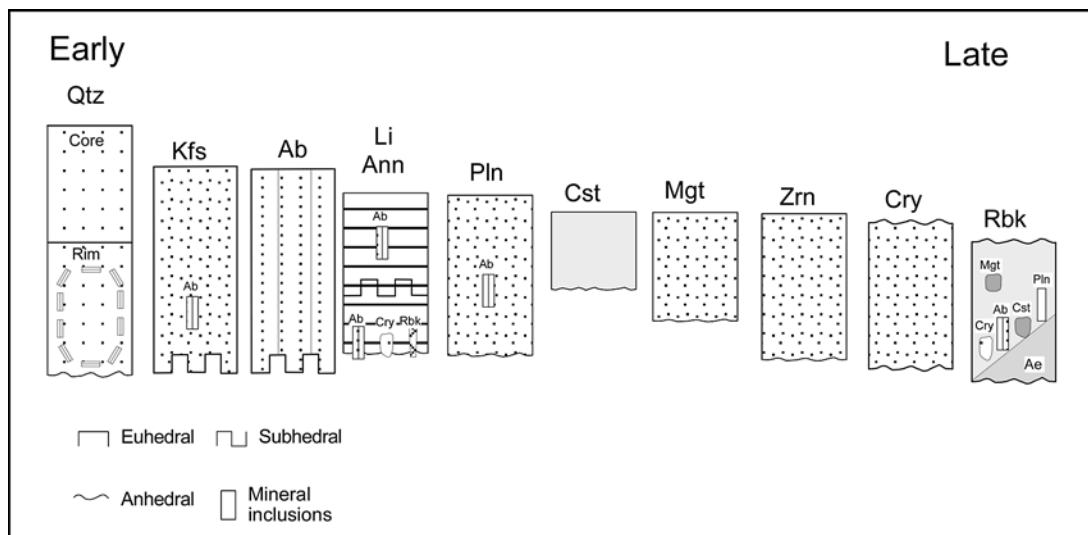


FIG. 4. Order of crystallization inferred for the albite-rich granite. Mineral symbols as in Kretz (1983) and Spear (1993); in addition, LiAnn stands for lithian annite.

(Figs. 5m, n) is found as large (>3 to 0.5 mm), euhedral, bipyramidal crystals with inclusions of albite, K-feldspar, fluorite, xenotime, and dust-sized opaque minerals. It is commonly corroded, with a homogeneous, recrystallized metamict core and a thin, clean, Hf-rich border zone (Figs. 6e, f). The transition from the peralkaline AbGC to the generally peraluminous AbGB is marked by: (1) replacement of cryolite by fluorite, (2) destabilization of micas and riebeckite and replacement by chlorite and iron oxides, (3) destabilization of the pyrochlore-group minerals and replacement by columbite, and (4) partial replacement of albite by quartz (Costi 2000). Geological and petrographic data indicate that the original magmatic mineral assemblage of the albite-rich granite core facies was destabilized and replaced along the margins and in the roof of the albite-rich granite body, leading to the formation of the AbGB.

#### MAGNETIC SUSCEPTIBILITY OF THE ALBITE-RICH GRANITE

Magnetic susceptibility (MS) values of the AbGC are moderately high (between  $0.255 \times 10^{-3}$  to  $64.4 \times 10^{-3}$ , with an average of  $4.2 \times 10^{-3}$  SIv) (Almeida 2002). This is compatible with the common presence of magnetite, the most abundant iron oxide mineral in the core facies. In contrast, the border facies is less magnetic (MS between  $1.61 \times 10^{-3}$  and  $1.94 \times 10^{-3}$ ,

average of  $1.77 \times 10^{-3}$  SIv; Almeida 2002); this reflects the intense replacement of magnetite by hematite during oxidation processes in the presence of a hydrothermal fluid phase.

The presence of primary magnetite in the AbGC suggests that the AbGC crystallized under relatively oxidizing conditions, possibly at or slightly above the NNO buffer. The destabilization of magnetite and its partial replacement by hematite in the AbGB facies indicates more oxidizing conditions (above the HM buffer) at the hydrothermal stage.

#### THE COMPOSITION OF MINERALS IN THE ALBITE-RICH GRANITE

##### Feldspars

Back-scattered scanning electron microscope studies (*cf.* Costi 2000) and electron-microprobe analyses of K-feldspar and albite of the core and border facies of the albite-rich granite show that feldspars in these rocks have compositions near their respective end-members (Table 2). Both feldspars have, however, high Fe contents (around 1 wt% Fe<sub>2</sub>O<sub>3</sub>, Table 2) and the K-feldspar is also enriched in Rb (ca. 2 wt% Rb<sub>2</sub>O; Table 2).

The chemical composition of the feldspars is shown in Or–Ab *versus* Fe<sub>2</sub>O<sub>3</sub> and Ab–An *versus* Fe<sub>2</sub>O<sub>3</sub> plots (Fig. 7; *cf.* Smith & Brown 1988). Both albite and K-feldspar are enriched in Fe<sub>2</sub>O<sub>3</sub> compared to common near end-member igneous alkali feldspars. Similar compositions or even more Fe-rich alkali feldspars are found in lamproites, carbonatites, and ultrapotassic rocks (Carmichael 1967, Smith & Brown 1988, Linthout & Lustenhouwer 1993, Kuehner & Joswiak 1996). Alkali feldspars in peralkaline granites are generally enriched in iron compared to those of metaluminous and peraluminous granites (Fig. 7). The K-feldspar from the albite-rich granite has a high Rb content and extremely low K/Rb ratio (Fig. 8a). Similar geochemical characteristics are found in the feldspars from the Tanco, Red Cross Lake (Černý *et al.* 1985b) and Volta Grande (Lagache & Quémeuneur 1997) pegmatites.

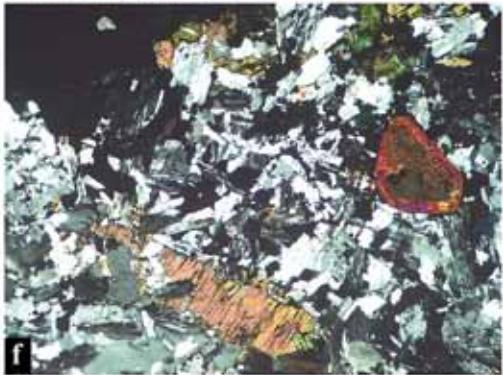
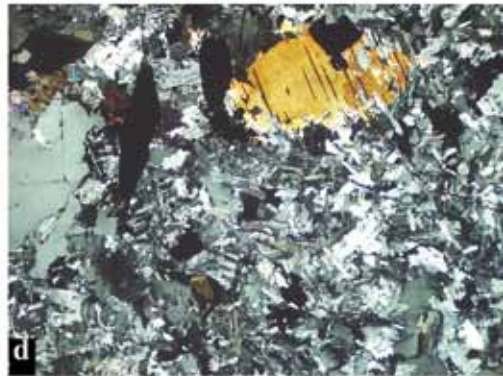
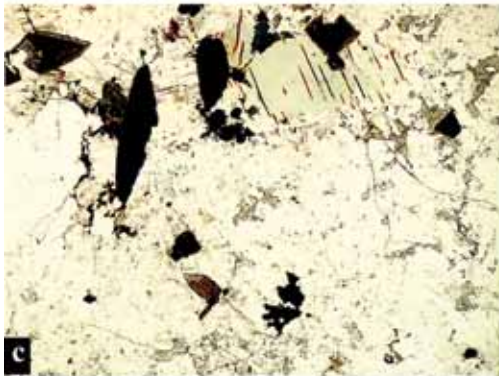
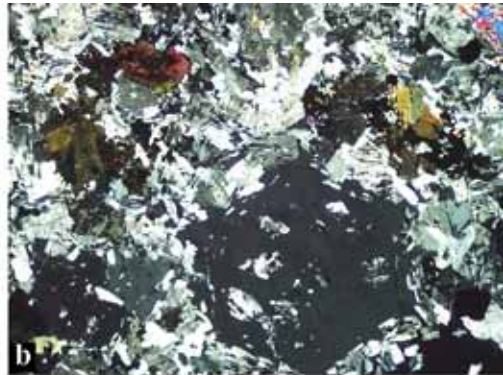
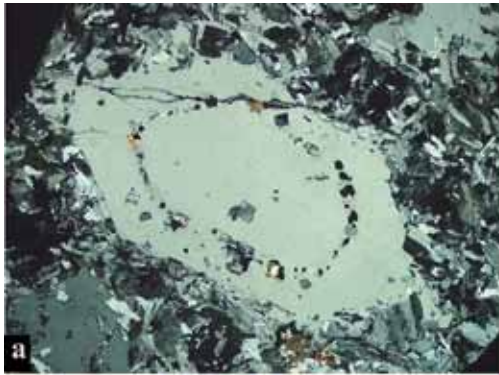
##### Micas

Two groups of trioctahedral Li–Fe micas are present in the AbGC (Table 3): an iron-rich mica, classified tentatively as zincian–rübidian–lithian annite (*cf.* Rieder *et al.* 1998) and zincian–rübidian polyolithionite. Both micas display extremely high Rb contents and very low K/Rb values (about 3 to 5). The K/Rb values of micas progressively increases from the equigranular core facies through the fluidal quartz syenitic rocks to the massive pegmatitic layers. In the latter rocks, which are located in the innermost part of the stock, micas are compositionally similar to the micas in rare-element

TABLE 2. REPRESENTATIVE COMPOSITIONS OF FELDSPARS FROM THE ALBITE-RICH GRANITE FACIES OF THE MADEIRA PLUTON

	Albite				K-feldspar			
	AbGC		AbGB		AbGC		AbGB	
SiO <sub>2</sub> wt%	68.63	68.81	68.67	68.65	64.25	64.13	63.54	63.83
Al <sub>2</sub> O <sub>3</sub>	18.48	18.54	18.37	18.41	17.35	17.26	17.43	17.77
CaO	0.01	0.00	0.00	0.02	0.00	0.00	0.00	0.00
MnO	0.00	0.00	0.00	0.00	0.03	0.00	0.02	0.01
FeO	1.10	0.95	0.99	1.12	0.72	0.59	0.69	0.36
SrO	0.00	0.00	0.00	0.00	0.00	0.00	0.00	0.00
BaO	0.06	0.00	0.00	0.23	0.00	0.00	0.00	0.00
Na <sub>2</sub> O	11.55	11.51	11.46	11.54	0.24	0.20	0.13	0.18
K <sub>2</sub> O	0.06	0.04	0.05	0.04	15.82	15.26	15.64	15.91
Rb <sub>2</sub> O	0.00	0.00	0.00	0.00	1.47	2.32	1.86	1.81
Sum	99.89	99.85	99.54	100.01	99.88	99.76	99.33	99.88
Si <i>apfu</i>	12.03	12.05	12.06	12.03	12.03	12.06	11.99	11.98
Al	3.82	3.83	3.80	3.80	3.83	3.83	3.88	3.93
Fe	0.16	0.14	0.14	0.16	0.11	0.09	0.11	0.06
Ca	0.002	0.00	0.00	0.004	0.00	0.00	0.00	0.00
Na	3.93	3.91	3.90	3.92	0.09	0.07	0.05	0.06
K	0.01	0.01	0.01	0.01	3.78	3.66	3.77	3.81
Mn	0.00	0.00	0.00	0.00	0.004	0.00	0.004	0.002
Rb	0.00	0.00	0.00	0.00	0.18	0.28	0.23	0.22
Ba	0.004	0.000	0.000	0.020	0.00	0.00	0.00	0.00
Sum	19.95	19.93	19.92	19.95	20.02	19.99	20.03	20.07
Ab mol. %	99.59	99.76	99.70	99.70	2.28	1.96	1.29	1.67
An	0.04	0.00	0.00	0.10	0.00	0.00	0.00	0.00
Or	0.37	0.24	0.30	0.21	97.72	98.04	98.71	98.33

AbGC: albite-rich granite, core facies; AbGB: albite-rich granite, border facies. The number of ions is calculated on the basis of 32 atoms of oxygen.



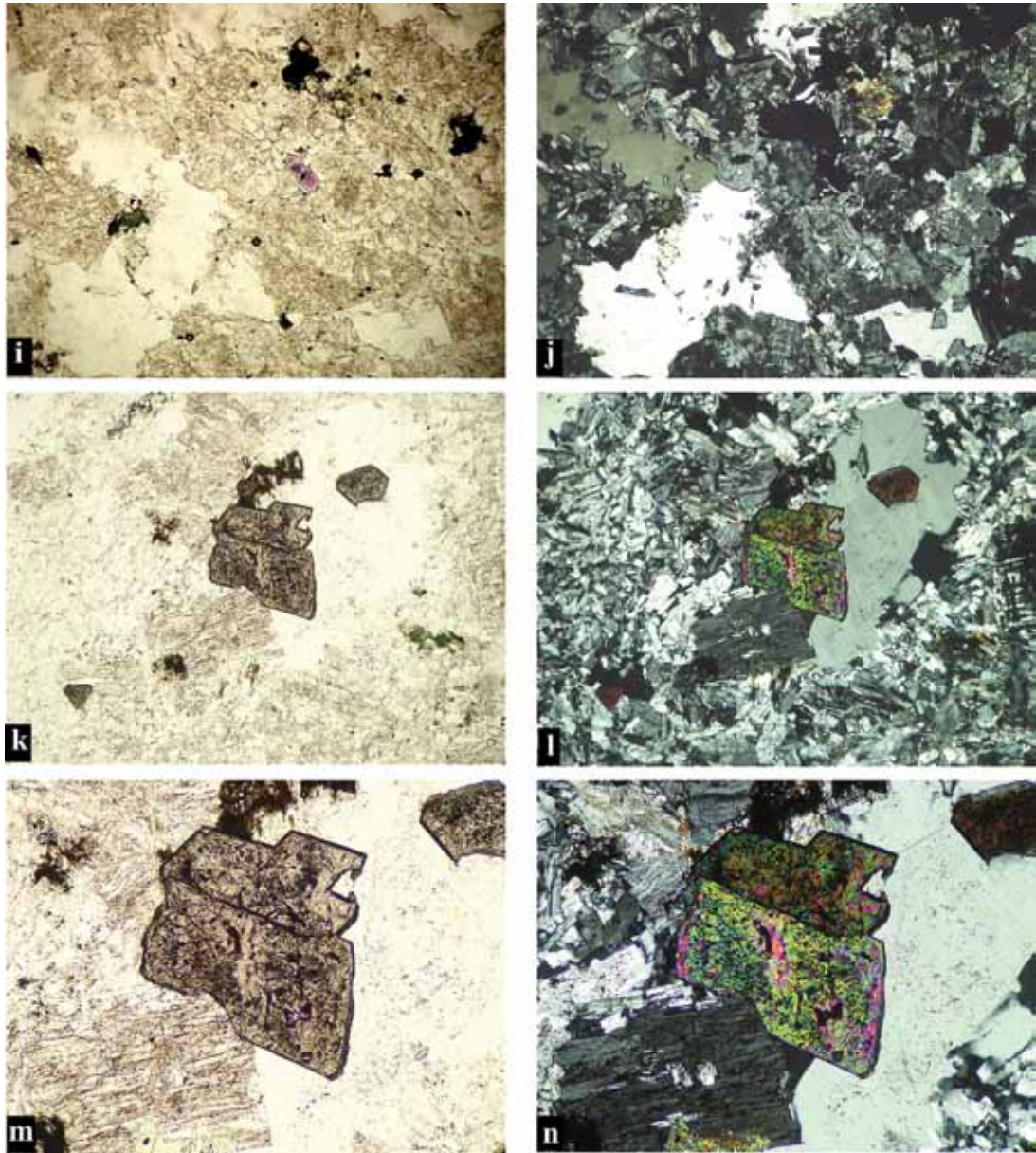
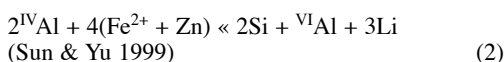
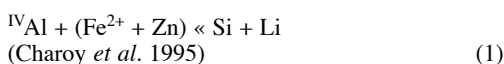


FIG. 5. Photomicrographs of essential and accessory minerals in the albite-rich granite. Albite granite, core facies. a) Euhedral snowball quartz phenocryst with inclusions of cryolite (black dots), polyolithionite (yellow) and albite. Matrix composed of albite laths, K-feldspar, and quartz (crossed nicols, width 7 mm). b) Basal section of quartz phenocryst with snowball albite and matrix of albite laths, K-feldspar and quartz, showing also agglomerate of riebeckite (left) and coarse zircon (top left) (crossed nicols, width 7 mm). c) Textural aspect of the albite-rich granite, core facies, showing (from top left to right) zircon, thorite and tabular bluish polyolithionite (with cleavages filled by reddish iron oxide), fine-grained cassiterite (lower center), and disseminated cryolite (colorless with moderate relief) (plane-polarized light, width 7 mm). d) Same point, crossed nicols. e) Coarse-grained aggregate and disseminated cryolite (top left and center), lithian annite and coarse-grained zircon with metamict, sieved core (plane-polarized light, width 3.5 mm). f) Same point, crossed nicols. g) Aspect of the albite-rich granite with a fluidal texture, showing disseminated cryolite (colorless, fine-grained), cassiterite (dark, fine-grained), riebeckite (dark, poikilitic, lower left corner) and elongate lamellae of lithian annite partially replaced by stilpnomelane (plane-polarized light, width 7 mm). h) Same point, crossed nicols. Albite-rich granite, border facies. i) Textural aspect of

the border facies, showing the clouded feldspars, anhedral quartz and a cavity filled by coarse quartz (center left), and opaque minerals, probably columbite (plane-polarized light, width 7 mm). j) Same point, crossed nicols. k) Cavity filled by coarse quartz (center) and partially included coarse zircon, without sieved core, (plane-polarized light, width 7 mm). l) Same point, crossed nicols. m) Detail of picture k, showing zircon crystal including fine-grained, metasomatic fluorite (plane-polarized light, width 3.5 mm). n) Same detail, crossed nicols.

pegmatites (Fig. 8b). A strong negative correlation ( $r = -0.94$ ) is observed between Fe and Zn in lithian annite, indicating a solid solution involving diadochy between these two elements. In polyolithionite, the relationship between Fe and Zn is more complex, but the compositions tend to show a positive correlation ( $r = 0.39$ ). The two groups of micas are F-rich, with F concentrations strongly increasing from the lithian annite to polyolithionite (respectively, ~4 to ~7 wt%; Table 3). The F concentrations in the lithian annite are higher in the pegmatitic zones (3.61 to 4.56 wt% F) than in the equigranular core facies (2.81 to 3.71 wt% F).

In the Li –  $R^{2+}$  – Al plot (Fig. 9; Foster 1960, Monier & Robert 1986), the micas of the albite-rich granite do not follow the classic polyolithionite – siderophyllite trend. They are more akin to Li–Fe–mica associated with pegmatites (Černý & Burt 1984). The polyolithionite compositions plot along the polyolithionite – annite trend and the lithian annite along the tainiolite – siderophyllite trend (Fig. 9). The evolution of both groups is controlled by the following coupled substitutions:

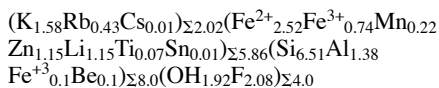


However, for the lithian annite, all Al is used in the sheets of tetrahedra, and there is no  ${}^{\text{VI}}\text{Al}$  available for the octahedra (Table 3). As a consequence, in the sheets of octahedra, Al should be replaced by  $\text{Fe}^{3+}$  in equation (2), resulting in the substitution:

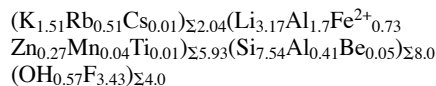


Representative formulae of the micas of the albite-rich granite are:

Lithian annite:



Polyolithionite:



A  $\text{Fe}_2\text{O}_3 / (\text{Fe}_2\text{O}_3 + \text{FeO})$  value of 0.25 was obtained by Mössbauer spectroscopy for the lithian annite of the pegmatitic zones (Costi 2000). However, SEM images show the presence of scattered very fine-grained magnetite and riebeckite inclusions in these micas (Figs. 6a, b) and it is likely that the value obtained does not reflect the contribution of the mica alone. Nevertheless, the relatively elevated iron-oxidation ratio is consistent with other indications suggesting relatively oxidizing

TABLE 3. REPRESENTATIVE COMPOSITIONS OF LITHIAN ANNITE AND POLYLITHIONITE FROM THE ALBITE-RICH GRANITE FACIES OF THE MADEIRA PLUTON

	LiAnn		Pln	
SiO <sub>2</sub> wt%	40.02	40.73	53.59	53.60
TiO <sub>2</sub>	0.56	0.38	0.11	0.09
SnO <sub>2</sub>	0.12	b.d.l.	0.02	0.06
Al <sub>2</sub> O <sub>3</sub>	6.72	5.67	12.41	12.46
MgO	b.d.l.	0.01	0.02	b.d.l.
CaO	b.d.l.	b.d.l.	0.02	b.d.l.
MnO	1.78	0.94	0.30	0.216
FeO	18.84	24.94	5.39	8.09
Fe <sub>2</sub> O <sub>3</sub> <sup>a</sup>	6.98	9.24	n.d.	n.d.
ZnO	8.87	2.48	2.55	1.23
PbO	b.d.l.	b.d.l.	1.36	b.d.l.
Na <sub>2</sub> O	b.d.l.	0.070	0.01	b.d.l.
K <sub>2</sub> O	7.66	8.09	8.21	8.46
Rb <sub>2</sub> O <sup>b</sup>	4.02	2.80	5.48	5.17
Cs <sub>2</sub> O <sup>b</sup>	0.34	0.04	0.25	0.31
F	4.01	4.23	7.26	6.98
Li <sub>2</sub> O <sup>c</sup>	1.93	2.14	5.83	5.83
BeO <sup>b</sup>	0.02	0.01	0.15	0.18
O = F	1.69	1.78	3.06	2.94
Sum	100.2	99.99	99.91	99.75
Si <i>apfu</i>	6.53	6.57	7.58	7.53
Be	0.01	0.00	0.05	0.06
Fe <sup>3+</sup>	0.16	0.35	-	-
<sup>VI</sup> Al	1.29	1.08	0.37	0.41
Σ T	8.00	8.00	8.00	8.00
<sup>VI</sup> Al	-	-	1.70	1.66
Ti	0.07	0.05	0.01	0.01
Sn	0.01	-	-	-
Mg	-	-	-	-
Mn	0.25	0.13	0.04	0.03
Fe <sup>3+</sup>	0.69	3.36	-	-
Fe	2.57	0.77	0.64	0.95
Zn	1.07	0.29	0.27	0.13
Pb	-	-	0.05	-
Li	1.27	1.39	3.32	3.30
Σ O	5.93	5.99	6.03	6.07
Ca	-	-	-	-
Cs	0.02	-	0.02	0.01
Na	-	0.02	-	-
K	1.59	1.66	1.48	1.52
Rb	0.42	0.29	0.50	0.47
Σ Interlayer	2.03	1.98	2.00	2.00
F	2.07	2.16	3.25	3.10
OH	1.93	1.84	0.75	0.90

LiAnn: lithian annite; Pln: polyolithionite. The number of ions is calculated on the basis of 22 atoms of oxygen (calculated OH = 4 – F). a: Fe<sub>2</sub>O<sub>3</sub> determined by Mössbauer spectroscopy; b: oxide determined by ion microprobe; c: Li<sub>2</sub>O calculated following Tindle & Webb (1990); b.d.l.: below detection limit, n.d.: not determined.

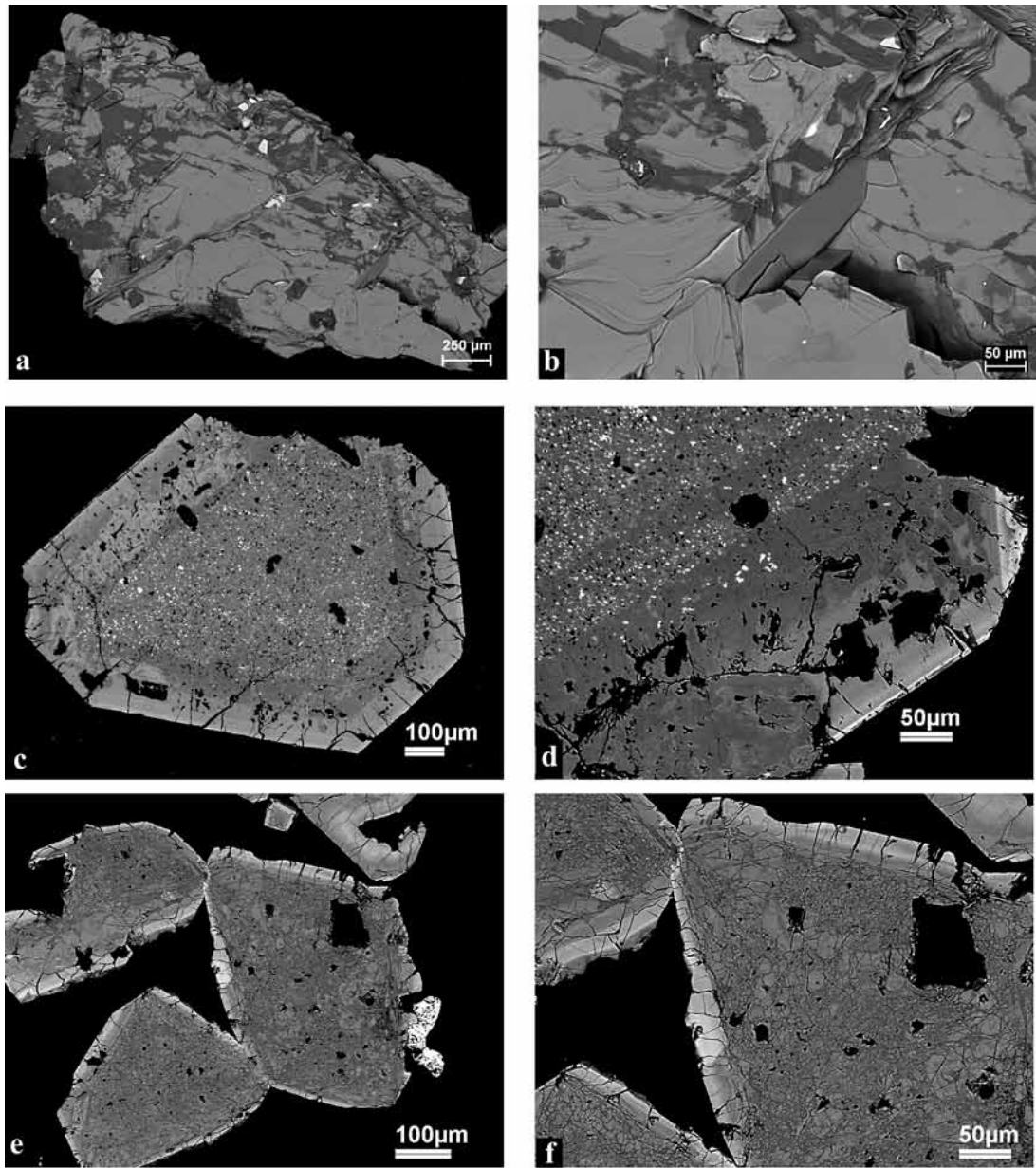


FIG. 6. SEM-BSE micrographs of mineral phases of the albite-rich granite. a) Fragment of massive mica showing lithian annite (light grey), polyolithionite (dark grey), octahedra of magnetite (bright) and riebeckite. b) Detail of a, showing the complex interdigitation of the micas and late, prismatic riebeckite. c) Zircon crystal from the albite-rich granite, core facies, showing the sieved core, with fine-grained thorite (bright) and a complex zoned, snowball border. d) Detail of the complex zoned border and a very thin, Hf-rich rim. e) Zircon crystal from the albite-rich granite, border facies, showing a recrystallized core with inclusions of albite, and a Hf-rich border rim. f) Detail of e.

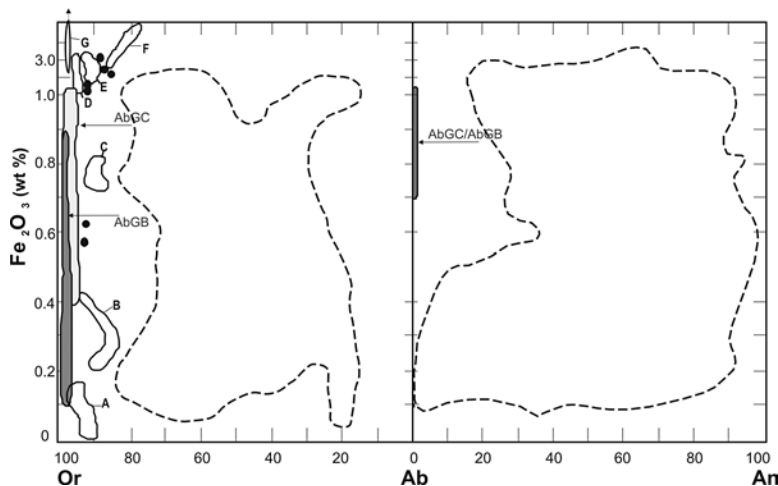
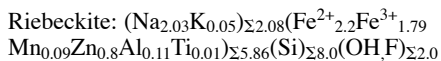


FIG. 7. Or–Ab–An versus  $\text{Fe}_2\text{O}_3$  diagram (modified from Smith & Brown 1988) for K-feldspar and albite from the albite granite facies. Dotted fields showing the Fe contents of feldspars from terrestrial volcanic rocks, as compiled by Smith & Brown (1988). Field A: K-feldspar in porphyritic granite, field B: K-feldspar in carbonatites, field C: K-feldspar in leucite-bearing lavas, field D: K-feldspar in lamprophyres, field E: K-feldspar in lamproites (for A through E see references in Smith & Brown 1988); field F: sanidine studied by Carmichael (1967), field G: field of sanidine studied by Kuehner & Joswiak (1996). Black dots: compositions of ferri-ferrous K-feldspar in Deer *et al.* 1963. AbGC: albite-rich granite, core facies; AbGB: albite-rich granite, border facies.

conditions during crystallization, such as the presence of magmatic magnetite and cassiterite (Linnen *et al.* 1996, Pichavant 1997) and the relatively high values of magnetic susceptibility (Almeida 2002).

#### Riebeckite and aegirine

The alkali amphibole found in the AbGC is a F-rich, zincian riebeckite (Table 4). Representative compositions of aegirine grains associated with riebeckite are also given (Table 4). Representative formulae of analyzed riebeckite and aegirine crystals are:

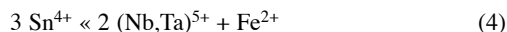


**Aegirine:**  $\text{Na}_{0.96}(\text{Fe}^{3+}_{0.81}\text{Fe}^{2+}_{0.11}\text{Al}_{0.1}\text{Ti}_{0.01})\Sigma_{1.03}(\text{Si})_{\Sigma 2.03}\text{O}_6$ . The amphibole shows strong variations in  $\text{FeO}^*$ ,  $\text{ZnO}$ , and  $\text{MnO}$  contents. Iron displays a negative correlation with ( $\text{ZnO} + \text{MnO}$ ). Riebeckite from the fluidal albite-rich rocks associated with the AbGC have the highest  $\text{FeO}^*$  and lower  $\text{ZnO}$  contents. The compositional evolution of riebeckite is thus similar to the evolution of lithian annite and polyolithionite (*i.e.*, compositions become progressively more evolved in the sequence core albite-rich granite – fluidal quartz syenitic rocks – massive pegmatitic layers). Thus,

compositions of solid-solution phases are controlled by internal processes of fractionation that involved the albite-rich granite as a whole.

#### Cassiterite

Cassiterite from the different facies of the albite-rich granite (Costi *et al.* 2000b, Table 4) has high  $\text{Nb}_2\text{O}_5$  and  $\text{Ta}_2\text{O}_5$ , low  $\text{TiO}_2$  and significant  $\text{FeO}$  (~0.45 wt%) contents. The dark-red or dark-brown core of the cassiterite crystals is enriched in  $\text{Nb}_2\text{O}_5$ ,  $\text{Ta}_2\text{O}_5$  and  $\text{FeO}$  (anal. AbGC1 and AbGB1 in Table 4). These oxides decrease regularly from the core through the red intermediate zone to the light red or colorless rim (anal. AbGC2 and AbGB2 in Table 4), where the lowest values are found. Note that  $\text{SnO}_2$  shows the opposite behavior, whereas  $\text{TiO}_2$  does not exhibit any significant variation. These data suggest that the main substitution mechanism in cassiterite is:



which is favored by relatively high temperatures during cassiterite crystallization (Möller *et al.* 1988).

The composition of cassiterite from the Madeira albite-rich granite is similar to that of magmatic cassiterite from evolved, topaz-bearing Finnish rapakivi gran-

ites (*cf.* Haapala 1997). Costi *et al.* (2000b) showed that the cassiterite of the albite-rich granite differs in composition from the hydrothermal cassiterite of greisens and episyenites associated with the Água Boa pluton which is comparatively impoverished in Nb, Ta, and Fe, and closer to end-member SnO<sub>2</sub> in composition. Thus the chemical data support the conclusion drawn from the textural data about the magmatic origin of cassiterite in the Madeira albite-rich granite (Costi *et al.* 2000b).

*Magnetite*

Reflected light microscopy and back-scattered scanning electron microscopy demonstrate that magnetite crystals in the Madeira albite-rich granite are homogeneous, lacking ilmenite exsolution lamellae. This, together with the absence of significant amounts of TiO<sub>2</sub> in the magnetite (EDS data), indicates that it has a near end-member composition. If it is assumed that magnetite is magmatic, as suggested by textural observations, then the absence of exsolved ilmenite suggests that magnetite crystallized below the magnetite-ulvöspinel

solvus at temperatures under 600°C (Burton 1991). This finding constrains the range of crystallization temperatures for the albite-rich granite itself.

GEOCHEMICAL FEATURES OF THE ALBITE-RICH GRANITE

The full geochemical data for granites of the Madeira suite will be scrutinized in a companion paper (Costi *et al.*, in prep.), but the essential aspects of the geochemistry of the albite-rich granite facies are summarized here (Table 5). The albite-rich granite core facies has SiO<sub>2</sub> contents of ~70 wt%, near the lower end of the range defined by the different facies of the Madeira granite (70–76 wt%, Table 5). The border

TABLE 4. REPRESENTATIVE COMPOSITIONS OF CASSITERITE, AEGIRINE AND RIEBECKITE FROM THE ALBITE-RICH GRANITE FACIES OF THE MADEIRA PLUTON

	Cassiterite				Aegirine		Riebeckite	
	AbGC <sup>1</sup>	AbGC <sup>2</sup>	AbGB <sup>1</sup>	AbGB <sup>2</sup>				
SiO <sub>2</sub> wt%	-	-	-	-	52.91	51.90	51.36	49.98
TiO <sub>2</sub>	0.09	0.03	0.10	0.07	0.41	0.37	0.06	0.04
Al <sub>2</sub> O <sub>3</sub>	-	-	-	-	1.68	0.80	0.59	1.14
FeO	1.62	0.17	1.81	0.72	28.68	31.01	30.63	30.32
MgO	-	-	-	-	0.01	b.d.l.	b.d.l.	b.d.l.
MnO	-	-	-	-	0.05	b.d.l.	0.68	1.12
CaO	-	-	-	-	0.01	b.d.l.	0.01	b.d.l.
Na <sub>2</sub> O	-	-	-	-	12.99	12.42	6.73	7.26
K <sub>2</sub> O	-	-	-	-	-	-	0.27	1.1
ZnO	-	-	-	-	-	-	6.10	3.10
F	-	-	-	-	-	-	0.53	1.38
Nb <sub>2</sub> O <sub>5</sub>	1.94	0.25	2.29	0.82	-	-	-	-
Ta <sub>2</sub> O <sub>5</sub>	0.39	0.00	0.30	0.16	-	-	-	-
SnO <sub>2</sub>	93.98	96.97	95.95	98.61	-	-	-	-
Sum	98.03	97.42	100.45	100.38	96.73	96.51	96.97	95.51
Si <i>apfu</i>	-	-	-	-	2.03	2.01	8.00	8.00
Ti	0.002	0.001	0.002	0.001	0.01	0.01	0.01	0.01
<sup>v</sup> Al	-	-	-	-	-	-	-	-
Fe <sup>3+</sup>	-	-	-	-	0.81	0.85	1.79	1.58
Sn	0.95	0.99	0.94	0.98	-	-	-	-
Nb	0.03	0.003	0.03	0.01	-	-	-	-
Ta	0.003	0.000	0.00	0.00	-	-	-	-
Fe <sup>2+</sup>	0.03	0.004	0.04	0.01	0.11	0.15	2.20	2.63
Zn	-	-	-	-	-	-	0.80	0.42
Mn	-	-	-	-	0.002	-	0.09	0.15
Mg	-	-	-	-	-	-	-	-
Ca	-	-	-	-	0.00	0.00	-	-
Na	-	-	-	-	0.96	0.93	2.00	2.15
<sup>40</sup> K	-	-	-	-	-	-	0.05	0.24
<sup>23</sup> Na	-	-	-	-	-	-	0.03	0.11
Sum	1.01	1.00	1.01	1.01	4.03	4.01	15.08	15.49

Mineral formulae calculated on the basis of two atoms of oxygen for cassiterite, and four cations for aegirine. The formulae of riebeckite were calculated with the software CLASAMPH (Currie 1997) on the basis of 15 atoms of oxygen, according to the procedure proposed by Leake *et al.* (1997); b.d.l., below detection limit. AbGC: albite-rich granite, core facies; AbGB: albite-rich granite, border facies; AbGC<sup>1</sup> and AbGB<sup>1</sup>: spot on the dark red core of the cassiterite crystal; AbGC<sup>2</sup> and AbGB<sup>2</sup>: spot on the light red to yellowish rim of the cassiterite crystal.

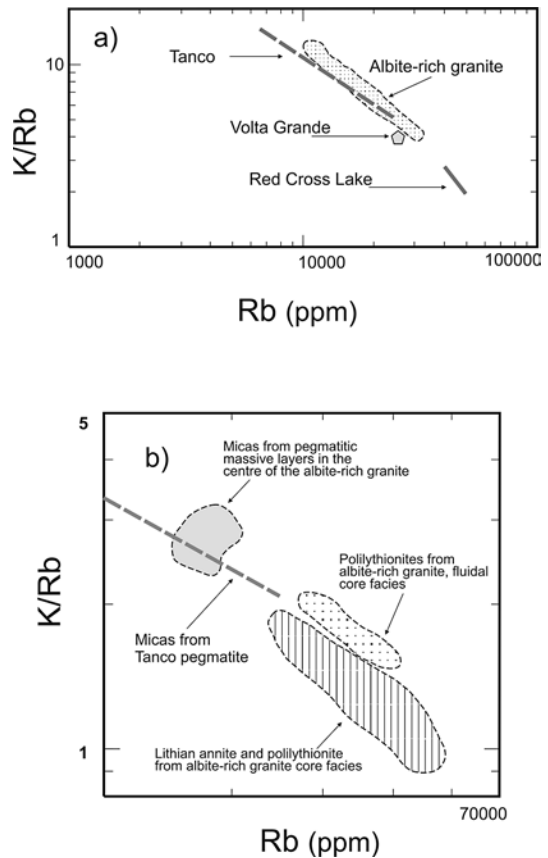


FIG. 8. (a) Rb versus K/Rb diagram for K feldspar of the albite-rich granite (dotted field) and the range displayed by K-feldspar from the Tanco, Red Cross Lake and Volta Grande pegmatites (see text for references). (b) Rb versus K/Rb diagram for the polythionite and lithian annite from the core facies and pegmatitic massive layers of the albite-rich granite and the range displayed by micas from the Tanco pegmatite.

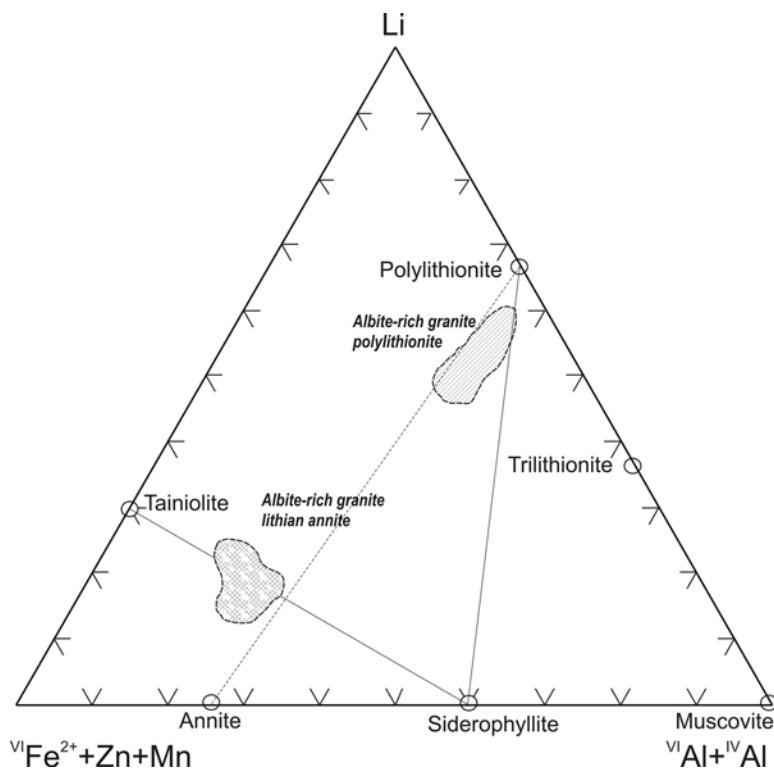


FIG. 9. Li – Al – R<sup>2</sup> diagram (modified from Monier & Robert 1986) for the lithian annite and polyolithionite from the albite granite, core facies. The end-member “siderophyllite 4” is from Sun & Yu (1999).

facies has higher and more variable SiO<sub>2</sub> contents. The core facies is peralkaline, whereas the border facies is metaluminous to peraluminous (Fig. 10a). For comparison, the amphibole–biotite syenogranite and biotite alkali feldspar granite of the Madeira pluton vary from metaluminous to slightly peraluminous, and the porphyritic hypersolvus alkali feldspar granite of Madeira and the Europa granite are chemically transitional between metaluminous and peralkaline (Fig. 10a). One critical difference in terms of major elements between the albite-rich granite core facies and the other types of granite in the Madeira pluton concerns Na<sub>2</sub>O, which is much higher in the core albite-rich granite than in all the other facies (e.g., ~6 wt% versus ~4 wt% Na<sub>2</sub>O, Table 5, Costi *et al.*, in prep.). As Al<sub>2</sub>O<sub>3</sub> remains almost constant and CaO contents are extremely low, the peralkaline character of the core facies (Figs. 10a, b) results directly from its elevated Na<sub>2</sub>O concentrations that are positively correlated with the amount of cryolite (Fig. 10c). The enrichment in Na<sub>2</sub>O in the albite-rich granite core facies is accompanied by a parallel enrichment in FeO<sub>t</sub>, which is typical of fractionation of silicic peralkaline systems (Scaillet & Macdonald 2003, Fig.

10d). In addition to the enrichment in Na<sub>2</sub>O and the depletion in CaO, the albite-rich granite core facies is strongly enriched in F (2–4 wt% F) and depleted in MgO and TiO<sub>2</sub> (Table 5).

In the normative CIPW diagram (Fig. 3b), the core facies samples plot at the low-temperature thermal valley of the Qtz–Ab–Or–H<sub>2</sub>O system (Tuttle & Bowen 1958). This region corresponds to F-rich residual magmatic liquids at equilibrium with quartz–feldspar assemblage at low pressures (Manning 1981). Samples from the equigranular albite-rich granite core facies define a compositional trend characterized by progressively increasing normative Ab and decreasing normative Qtz at nearly constant normative Or (Fig. 3b). They mimic the displacement of minima and eutectic points with the progressive addition of F in the haplogranite system (Manning 1981, Pichavant & Manning 1984), strongly suggesting, therefore, that the rocks of the core facies represent products of crystallization of F-rich magmatic liquids. The “quartz syenitic” fluidal rocks have normative Ab and Qtz respectively higher and lower than the equigranular rocks of the core facies. They plot near the Ab-rich end of the general trend

(Fig. 3b). In comparison, samples of the border facies cluster near the center of the Qtz–Ab–Or diagram (Fig. 3b), and their compositions do not correspond to F-rich magmatic liquids (Manning 1981).

The albite-rich granite also shows extremely elevated contents of high-field-strength (HFSE) elements such as Zr, Nb, Sn, Hf, Ta and Th (Costi *et al.*, in prep.). Enrichment in these elements goes along with progressive differentiation (Fig. 10b), and this can be explained by the combined influence of the peralkaline composition of the melt and elevated F concentrations in it, favoring the concentration of HFSE (Collins *et al.* 1982, Černý *et al.* 1985a, Whalen *et al.* 1987, London *et al.* 1989, Taylor 1992, Keppler 1993, Linnen 1998).

## DISCUSSION

### *Relative importance of magmatic and hydrothermal processes in the petrogenesis of the Madeira albite-rich granite*

Costi *et al.* (2000a) concluded that the albite-rich granite and porphyritic hypersolvus alkali feldspar granite of the Madeira pluton are coeval; contact relationships indicate that these granites were derived from liquids that coexisted during at least part of their crystallization history. Petrographic data favor a magmatic origin for the AbGC. The similar modal proportions of quartz, K-feldspar and albite, the clustering of AbGC samples in the Qtz–Kf–Ab modal plot (Fig. 3a), the snowball textures, contact relationships between different minerals, and the proposed sequence of crystallization for the AbGC are difficult to reconcile with a secondary (*i.e.*, metasomatic) origin (Horbe *et al.* 1991). The relative proportions of quartz and feldspars (Table 1), and their respective grain-size (Costi 2000) suggest that the textural evolution of the albite-rich granite was controlled by near-cotectic crystallization (Fig. 3c). This interpretation is supported by the normative composition of the core-facies samples, which complies with the composition of low-pressure silicic liquids enriched in F (Fig. 3b). In contrast, the AbGB are significantly different from the AbGC. The textural and mineralogical changes observed in this facies, compared to the AbGC (Table 1), and the differences in modal composition between the two facies, indicate that the present AbGB composition is not primary, but rather the result of a pervasive hydrothermal episode (Costi 2000).

The fact that albite and K-feldspar in the albite-rich granite show almost end-member compositions implies that feldspar compositions have re-equilibrated at low subsolidus temperatures. However, this does not necessarily imply that the feldspars were totally recrystallized under the influence of secondary hydrothermal processes. Signs of albite exsolution are lacking in K-feldspar, and intergranular albite crystals have not been observed in the albite-rich granite. Both feldspars have high concentrations of Fe and the K-feldspar

show elevated values of Rb (Table 2). These elements are present in solution in the feldspars, and not as components of exsolved micrograins or inclusions, and therefore the composition of feldspars reflects crystallization under specific conditions. Feldspars from ultrapotassic and peralkaline magmatic rocks are characterized by high Fe<sub>2</sub>O<sub>3</sub> (Smith & Brown 1988). The K/Rb values indicate that the K-feldspar from the albite-rich granite is very similar to that crystallized from rare-element-enriched pegmatite-forming melts (Černý *et al.* 1985b). This, together with the similarity noted between compositions of micas in the albite-rich granite and in rare-element pegmatites (Fig. 8b), suggests that the melt involved with the Madeira albite-rich granite was extremely evolved. The progressive compositional evolution of amphibole and micas from the equigranular core facies to the fluidal rocks and the pegmatitic zones is consistent with a mechanism of internal fractionation

TABLE 5. REPRESENTATIVE COMPOSITIONS OF THE EUROPA PLUTON AND VARIOUS FACIES OF THE MADEIRA PLUTON

Rock	EUG	ABSG	BAFG	PHG	AbGC			AbGB	
Sample	189	125	193	191	82a	121	127	93-A	157
SiO <sub>2</sub> wt%	75.94	70.4	74.46	74.11	68.55	71.75	66.80	70.68	75.87
Al <sub>2</sub> O <sub>3</sub>	11.73	13.0	12.79	12.56	13.08	12.78	14.94	12.61	12.20
FeO	1.23	2.5	1.08	1.01	0.86	0.79	1.88	2.13	0.28
Fe <sub>2</sub> O <sub>3</sub>	1.29	2.1	0.58	1.36	1.74	1.55	1.18	1.44	2.29
CaO	<0.10	1.3	0.81	0.72	<0.05	0.08	0.03	1.02	0.64
MgO	<0.10	0.28	<0.10	<0.1	0.02	0.04	0.25	0.08	0.10
MnO	<0.03	0.16	<0.03	0.03	0.05	0.05	0.04	0.09	0.02
Na <sub>2</sub> O	4.14	3.8	3.83	4.05	6.98	5.88	5.39	3.72	3.78
K <sub>2</sub> O	4.74	5.1	5.23	4.81	4.02	4.39	4.49	4.84	4.88
TiO <sub>2</sub>	0.18	0.47	0.15	0.15	0.03	<0.03	0.05	0.06	tr.
P <sub>2</sub> O <sub>5</sub>	<0.05	0.13	0.05	<0.0	0.05	0.02	0.06	0.07	0.05
L.O.I.	0.39	0.41	0.62	0.86	2.14	1.91	1.89	0.85	0.51
Sum	99.58	100.33	99.60	99.66	97.52	99.24	97.00	97.59	100.42
Ba ppm	27.5	695	258	66	4.6	6.5	19	15	30.7
F	1400	1250	6800	6000	32300	28100	17000	7000	3500
Ga	43.4	19	24	43	67.8	67	75.1	67.5	58
Hf	29.2	14	9.14	20.8	31.3	37.3	21.6	42.0	21.5
Li	103	10	270	369	964	789	992	32	4
Nb	69.4	32	48.4	66.4	126.5	117.4	250.4	143.5	90.0
Rb	388	267	1334	1497	5266	6944	7538	4070	1870
Sn	20.3	36	11.7	20.8	2194	1310	1319	2504	600
Sr	<4	101	28.9	16.2	0.59	<0.5	5.65	18.3	5.4
Ta	5.93	<5	5.08	4.6	198	237	283	250	156
Th	44.2	31	146	113	1169	897	447	336	151
U	11.5	<10	26.8	16.1	359	241	721	136	104
Y	100	134	125	167	90.5	200	191	204	101
Zn	241	172	112	297	1242	1740	3068	1276	679
Zr	903	532	254	534	5137	2970	1977	4865	2511
La	91.0	75.5	75.6	115	18.38	24.9	169.1	27.77	14.10
Ce	182.0	171.7	154	237	72.28	98.4	399.1	95.44	60.90
Pr	22.4	*	17.3	27.5	8.66	11.3	64.01	11.35	7.06
Nd	81.7	63.7	55.2	95.9	23.14	31.8	142.9	31.16	18.1
Sm	20.3	13.5	10.7	22.3	12.16	17	45.82	18.51	8.94
Eu	0.40	1.45	0.51	0.91	0.28	0.37	0.93	0.43	0.25
Gd	18.8	9.41	9.22	20.3	11.2	17.8	32.75	19.35	7.9
Tb	3.36	*	2.08	4.05	4.29	7.17	10.4	8.22	3.34
Dy	20.0	8.25	16.9	28.00	35.57	66.9	78.71	69.88	29.90
Ho	3.92	1.56	4.11	6.18	8.65	15.60	16.49	15.62	8.07
Er	11.5	3.78	16.00	21.4	29.88	56.00	51.92	52.7	31.8
Tm	1.79	*	3.57	4.18	7	11.1	11.03	12.35	7.31
Yb	12.8	3.27	27.00	31.3	50.78	73.8	74.6	88.93	55.3
Lu	1.90	0.411	4.12	4.6	7.78	9.82	11.18	12.88	7.82

EUG: Europa pluton; Madeira pluton: ABSG: amphibole–biotite syenogranite, BAFG: biotite – alkali feldspar granite, PHG: porphyritic hypersolvus granite, AbGC: albite-rich granite, core facies, AbGB: albite-rich granite, border facies. \* Element not sought.

involving the body of the sodic felsic magma as a whole. The high contents of Nb, Ta, and Fe in cassiterite from the albite-rich granite (Möller *et al.* 1988, Neiva 1996, Haapala 1997) and the compositional differences between cassiterite in the albite-rich granite and in the greisens and episyenites imply that cassiterite composition is rather controlled by relatively high-temperature than low-temperature processes.

In conclusion, all the aspects above demonstrate that the essential features of the Madeira albite-rich granite are magmatic in origin. In this respect, the Madeira albite-rich granite is similar to many other sodic leucogranites (Kovalenko & Kovalenko 1984, Pichavant *et al.* 1987, London *et al.* 1989, Cuney *et al.* 1992, Taylor 1992, Xiong *et al.* 1999, Lukkari & Holtz 2007). The mineralogical and petrographic data, the position of the AbGB in the top part or along the border zones of the albite-rich granite sheet, and the gradual transition between the border and the core facies strongly suggest

that the AbGB was initially similar to the AbGC, and that it has been subsequently modified by autometasomatic processes. The AbGB thus represents a locally altered, strongly oxidized equivalent of the AbGC.

#### *The role of F in the evolution of the Madeira albite-rich granite*

Much experimental work has been carried out to evaluate the influence of F on the crystallization of felsic granitic systems. The first studies (Wyllie & Tuttle 1961, Glyuk & Anfilogov 1973, Kovalenko 1978) revealed a strong decrease in the liquidus and solidus temperatures of the system Qtz–Ab–Or–H<sub>2</sub>O (Tuttle & Bowen 1958) with the addition of F. Later, detailed melting and crystallization experiments on either synthetic systems or natural F–Li-rich granites and pegmatites (Manning 1981, Pichavant & Manning 1984, Weidner & Martin 1987, Pichavant *et al.* 1987,

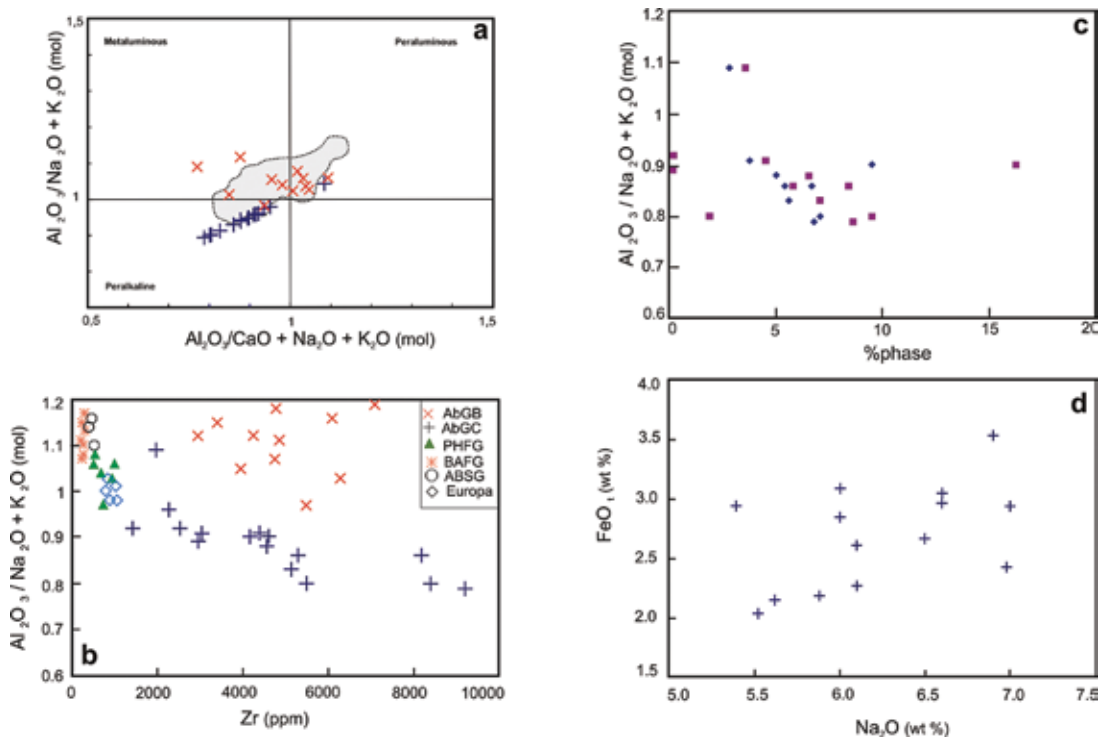


FIG. 10. Geochemical plots for the Madeira and Europa plutons. a) diagram A/NK versus A/CNK (molar ratios) for the Madeira pluton; the light grey field is occupied by the samples of the amphibole-biotite syenogranite, biotite-alkali feldspar granite and porphyritic hypersolvus alkali feldspar granite. b) A/NK (molar ratio) versus Zr (in ppm) for the facies of the Madeira and Europa plutons. c) A/NK (molar ratio) versus modal contents of cryolite (filled square) and the sum of modal cryolite plus riebeckite plus aegirine (filled diamonds) for the albite-rich granite, core facies of the Madeira pluton. d) FeO<sub>1</sub> versus Na<sub>2</sub>O (wt%) for the albite-rich granite, core facies of the Madeira pluton. Abbreviations in the inset: Europa: Europa pluton, ABSG: amphibole-biotite syenogranite, BAFG: biotite-alkali feldspar granite, PHFG: porphyritic hypersolvus alkali feldspar granite, AbGC: albite-rich granite, core facies, AbGB: albite-rich granite, border facies.

Manning & Pichavant 1988, London 1992, Xiong *et al.* 1999, 2002, Veksler & Thomas 2002, Veksler *et al.* 2002, Lukkari & Holtz 2007) have confirmed the early interpretations. These studies have validated the interpretation of mineralized, F–Li-rich albite granites as products of magmatic crystallization, regardless of the fact that they are commonly affected by late- or postmagmatic processes. The presence of F also promotes the transition from hypersolvus to subsolvus conditions during magmatic crystallization at low pressures in Ca-free (or Ca-poor) systems (Manning 1981). Consequently, fractionated albite-rich granites are usually characterized by the presence of two feldspar phases, an essentially albitic one and a dominantly potassic one. The presence of F has a strong influence on the physical properties of granitic melts. This includes depolymerization and reduction of the melt viscosity (Dingwell 1988, Johannes & Holtz 1996, Dingwell *et al.* 1998, Lukkari & Holtz 2007), vesiculation and degassing processes, and partitioning of H<sub>2</sub>O and halogens between fluid and melt (Webster 1990, London 1992, Dingwell *et al.* 1998, Webster & Rebbert 1998).

The general conclusions from the experiments quoted above can be directly applied to the Madeira albite-rich granite. However, it is worth pointing out that almost all of the works mentioned deal with metaluminous to peraluminous systems or rocks and, in this aspect, are different from our granite, which is peralkaline. Nevertheless, the high F content of the Madeira albite-rich granite is consistent with its subsolvus character and explains the extreme enrichments observed in HFSE, Li, Cs, Rb and other elements. Deposits of tin and related rare metal (Ta, Nb, Li, Be, Zr, and REE) are also commonly associated with F-rich granites. However, Sn is not usually found concentrated in peralkaline granites at economic levels (Bowden & Kinnaird 1984, Kinnaird *et al.* 1985, Pollard 1995). In this aspect, the Madeira albite-rich granite is an unusual example of an evolved granite.

For F-rich granite systems, experimental studies have indicated solidus temperatures around 550°C (Kovalenko 1978, Manning 1981, Pichavant *et al.* 1987, Lukkari & Holtz 2007) or even ~530 to 500°C (Xiong *et al.* 1999, 2002). These latter temperatures are probably good estimates of the solidus for the Madeira albite-rich granite. They contrast with temperatures around 700 Å 50°C obtained experimentally for the solidus of low-F peralkaline felsic magmas at 150 MPa (Scaillet & Macdonald 2001). The liquidus temperatures are also reduced but the effect of increasing F content on the liquidus temperature for a given composition depends on the composition involved (Manning 1981). Liquidus temperatures around 750 to 700°C in F-bearing leucogranite systems have been generally obtained (Manning 1981, Pichavant *et al.* 1987, Johannes & Holtz 1996, Xiong *et al.* 1999, 2002, Lukkari & Holtz 2007). These can be considered as the maximum estimates of the liquidus temperature of the Madeira albite-rich granites.

### *Origin of the Madeira albite granite*

Probably the most striking aspect of the Madeira albite-rich granite is its bulk peralkaline character, and the coexistence in the same granite stock of magmatic phases that are not usually found together. For example, the presence, in the albite-rich granite, of mineral phases typical of peralkaline granites such as riebeckite, aegirine, cryolite and pyrochlore, side by side with phases characteristic of peraluminous systems such as polyolithionite, is not common even in evolved granitic systems. In the same way, cassiterite is not usually found strongly concentrated in peralkaline granites (Bowden & Kinnaird 1984, Kinnaird *et al.* 1985, Pollard 1995). The exceptionally high modal contents of zircon, as well as the presence of thorite, are also noteworthy, because peraluminous albite granites have low to very low modal amounts of zircon, and they typically lack thorite. However, in the Madeira albite-rich granite, the abundance of these minerals is consistent with its peralkaline character. Lenharo *et al.* (2003) calculated zircon-saturation temperatures for different facies of the Madeira pluton, but noted problems with temperature estimates for the albite-rich granite because of its very high Zr contents and peralkaline character.

The peralkaline character of the Madeira albite-rich granite, the crystallization of mineral phases typical of peralkaline magmas, and elevated HFSE concentration levels all suggest that the albite-rich granite originated from a peralkaline and also F-rich silicic melt. However, almost all F-rich albite granites worldwide are peraluminous and, thus, the Madeira albite-rich granite, if crystallized from a parental peralkaline melt, would represent an unusual case. One critical question is whether the melt parental to the albite-rich granite was *initially* peralkaline. Alternatively, the peralkaline character may have developed relatively *late* during differentiation of a metaluminous to slightly peraluminous magma (possibly similar to the biotite alkali feldspar granite) or of a metaluminous to peralkaline magma (like the porphyritic hypersolvus granite; see discussion below).

Mineral phases typical of peralkaline systems (riebeckite, aegirine), are present in the albite-rich granite. However, as commonly observed in peralkaline granites, these phases are relatively late in the crystallization sequence (Fig. 4), the main early crystallizing phases in the albite-rich granite being quartz, the feldspars and micas. There is no evidence for the early crystallization of such phases as iron-rich clinopyroxene or calcic amphibole (ferrorichterite) that are typical of the crystallization sequence of peralkaline rhyolites (Scaillet & Macdonald 2003). However, this can be due to the extremely low CaO contents of the albite-rich Madeira granite. In their experiments, Scaillet & Macdonald (2003) found that sodic amphibole (arfvedsonite) is restricted to near or below the solidus, whereas above the solidus, amphibole is sodic–calcic.

This is consistent with the late appearance of sodic amphibole (riebeckite) in the Madeira albite-rich granite. Feldspar compositions and, in particular, their high concentrations of  $\text{Fe}^{3+}$ , are consistent with growth in a peralkaline environment (Smith & Brown 1988). However, feldspars in the albite granite continuously re-equilibrated down to solidus or subsolidus conditions (see above) and, therefore, they provide little indication on early conditions of crystallization. We conclude that the mineralogical data provide no decisive support for an early peralkaline parental melt.

The concentrations of  $\text{FeO}_t$  in the Madeira albite-rich granite range from around 2 to 3.5 wt% and are much higher than in peraluminous albite granites (Štemprok & Šulcek 1969, Pichavant *et al.* 1987, Huang *et al.* 2002, Badanina *et al.* 2004, Webster *et al.* 2004). Whole-rock  $\text{FeO}_t$  concentrations increase with decreasing A/NK and increasing Zr (Fig. 10d). There is also a slight decrease of  $\text{Al}_2\text{O}_3$  at increasing  $\text{FeO}_t$  contents. Overall, this differentiation scheme is strongly unusual for metaluminous or peraluminous silicic magmas (*cf.* Pichavant *et al.* 1987, Rämö 1991, Frost *et al.* 2002, Dall'Agnol *et al.* 2005, Dall'Agnol & Oliveira 2007). However, differentiation in peralkaline compositions, especially under relatively reducing conditions, may produce such a fractionation pattern (Scaillet & Macdonald 2003). During experimental crystallization of peralkaline rhyolites, these authors observed a progressive increase in  $\text{FeO}_t$ , concomitant with a decrease of  $\text{Al}_2\text{O}_3$  and A/NK in the residual melt. Therefore, the major-element fractionation patterns of the Madeira albite-rich granite are consistent with differentiation in a peralkaline environment. Yet, no clear evidence is provided for peralkaline conditions early in the differentiation history. The same conclusion applies to trace elements. The presence of exceptionally elevated HFSE concentration levels in the albite-rich granite reflects the enhanced transport properties for HFSE in peralkaline and F-rich melts, but they do not require that peralkaline and F-rich conditions appropriate for the solution of HFSE were established early in the system.

On a regional scale, the Madeira albite-rich granite is the only granitic rock showing a strongly peralkaline character. Most A-type granites in the Madeira suite are either metaluminous or peraluminous, and the porphyritic hypersolvus alkali feldspar granite from the Madeira pluton and the Europa granite are transitional between metaluminous and peralkaline (Fig. 10a). Although a mantle source has been commonly proposed for peralkaline granites (Baker & McBirney 1985, Nardi & Bonin 1991, Bonin 1996), Nd isotope data suggest that the different facies of the Madeira pluton, including the albite-rich granite, have a crustal source of Paleoproterozoic age (Costi *et al.* 2000a, in prep., Lenharo *et al.* 2003). This reduces the possibility of a mantle origin of the albite-rich granite, and reinforces the hypothesis

that the different granitic units of the Madeira pluton have broadly similar sources. Therefore, if the parental melt of the Madeira albite-rich granite was originally peralkaline, similar crustal sources must have been able to generate silicic melts with a wide range of A/NK (from ~0.8 for the albite-rich granite to nearly 1.2 for the amphibole–biotite and biotite alkali feldspar granites, Fig. 10b). However, it is hardly possible to vary the A/NK of silicic partial melts generated from the same crustal source. Moreover, no experimental study of crustal anatexis has yet produced peralkaline melts, although the breakdown of clinopyroxene during partial melting of quartzofeldspathic sources has been suggested as a possibility (*e.g.*, Scaillet & Macdonald 2003).

Given the lack of supporting mineralogical and geochemical evidence and the difficulties with the crustal generation of peralkaline silicic melts, we conclude that the parental melt of the Madeira albite-rich granite most probably was not originally peralkaline. This leaves the possibility, discussed in detail below, that a transition to peralkaline conditions occurred during the course of magmatic differentiation.

#### *Late-stage evolution of peralkalinity*

Melt-inclusion studies of highly evolved tin-rich granitic magmas (Thomas *et al.* 2005, 2006, and references therein) have emphasized the importance of immiscibility processes in the final stages of evolution of F-, B- and P-rich metaluminous to peraluminous leucogranite melts. Thomas *et al.* (2006) presented strong evidence that a F-rich evolved peraluminous magma can generate two different melts, one peralkaline and the other peraluminous, by immiscibility processes. The peralkaline phase is enriched in alkalis, Cl, P, B, F, Ca, Fe, and HFSE (Sn, W, Nb, Ta, Zr) and depleted in Si and Al in comparison with bulk-rock granite or the peraluminous phase (Thomas *et al.* 2006). The peralkaline melts are rarely preserved in nature (except as melt inclusions) because, in general, intense greisenization, reactions between peralkaline and peraluminous host rocks, and loss of alkalis by vapor-phase separation and degassing will remove evidence for the presence of the peralkaline melt. Unusual associations of minerals including nepheline, diopside, kalsilite, cryolite, leucite, and aegirine (among other phases) may coexist with peralkaline melt inclusions as crystalline remnants of the peralkaline evolution (Thomas *et al.* 2006). For example, cryolite is found together with nepheline, Rb-rich leucite and other accessory phases in the topaz–albite granites of Zinnwald; in the Ehrenfriedersdorf pegmatites, aegirine and kalsilite form exsolution textures after nepheline (Thomas *et al.* 2006).

Thomas *et al.* (2006) emphasized immiscibility as the main process responsible for the generation of

the peralkaline phase, and interpreted the peralkaline inclusions as melts. However, one critical characteristic of the peralkaline fraction is its H<sub>2</sub>O content, very elevated, with up to more than 50 wt% H<sub>2</sub>O in some cases (Thomas *et al.* 2006). As a consequence, the density of the peralkaline phase approaches values as low as 1–1.5 g/cm<sup>3</sup> (Thomas *et al.* 2006). In our view, these characteristics make the peralkaline fraction more akin to a dense silicate-rich aqueous fluid rather than of a melt phase (see also Preston *et al.* 2003). In other words, the phase separation process identified by Thomas *et al.* (2006) should not be mistaken with anhydrous liquid–liquid immiscibility, as observed in silicate–fluoride systems (Dolejs & Baker 2007a, b). Yet, the existence of a late-stage peralkaline phase in the differentiation of evolved granitic magmas seems firmly established (Thomas *et al.* 2006).

In Pitinga, no melt-inclusion data are available. However, the mineralogical and geochemical evidence outlined above clearly demonstrates that peralkaline conditions prevailed during late-stage crystallization. In fact, the bulk peralkaline character of the albite-rich granite and the elevated (at the wt% level) modal proportions of cryolite in the granite (Table 1, Fig. 10c) show that the imprint of a peralkaline evolutionary stage is much more developed at Pitinga than in the Erzgebirge examples described by Thomas *et al.* (2006). Yet, analogies between the Madeira albite-rich granite and the Erzgebirge mineral phases and melt inclusions are remarkable. These include: cryolite, generally found in the crystalline remnants of the peralkaline evolution of these extremely evolved melts, an important modal phase in the Madeira albite-rich granite; cassiterite, an ubiquitous accessory mineral in the Madeira albite-rich granite, also present in the peralkaline zones associated with the Ehrenfriedersdorf tin-rich granite; the peralkaline melt-inclusions from Zinnwald contain high concentrations of, *e.g.*, Sn and Nb (Thomas *et al.* 2006). This is compatible with the unusual association of cassiterite and pyrochlore in the Madeira albite-rich granite (Table 1); both minerals are found in significant amounts and are exploited at the Pitinga mine. Zircon is an exceptionally abundant accessory mineral in the Madeira peralkaline albite-rich granite (1.1 vol.% as an average content; Table 1) and shows textural features similar to those observed in the solid phases found in the melt inclusions of Erzgebirge (Thomas *et al.* 2006), suggesting similar conditions of crystallization for both magmas. Xenotime is found in the pegmatites associated with the Madeira albite-rich granite and is also present in the peraluminous and peralkaline environments of highly evolved tin-rich granites (Thomas *et al.* 2006).

We propose that the peralkaline phase at Pitinga resulted from a phase-separation process similar to that identified in the Erzgebirge examples. This peralkaline phase separated at some point of the evolution

of a parental magma that was most probably slightly peralkaline to metaluminous, similar to the porphyritic hypersolvus alkali feldspar granite. In this model, the A/NK *versus* Zr whole-rock evolution (Fig. 10b) can be interpreted as a two-component mixing trend between (1) a magmatic end-member (A/NK  $\approx$  1, Zr  $\leq$  1000 ppm), marked by the early assemblages of the albite-rich granite, and (2) a peralkaline end-member phase (A/NK  $<$  0.8, Zr  $\geq$  1000 ppm), having the physical and chemical properties outlined above, and whose crystallization yielded, among other phases, cryolite, riebeckite, aegirine, and most of the HFSE minerals. Note that the samples of the albite-rich granite core facies would correspond to mixtures in varying proportions between the two poles (Fig. 10b). Thus, the peralkalinity is not constant from one rock to the other, but varies along with the local proportion of end members in the rock. In Figure 10b, the porphyritic hypersolvus alkali feldspar granite and the Europa granite would plot closer to the inferred magmatic end-member. Samples from the border facies would represent rocks where the imprint of the peralkaline phase has been erased during secondary hydrothermal processes.

The Madeira albite-rich granite thus constitutes a rare example of Nb–Sn–Zr-mineralized albite-rich granite characterized by both an intense development and the remarkable preservation of a peralkaline evolutionary stage. This peralkaline stage, which has been identified in F-, B- and P-rich metaluminous to peraluminous leucogranitic melts (Thomas *et al.* 2006), results from a phase-separation process giving rise to a hydrous, F-rich, peralkaline phase having the ability of transporting and concentrating HFSE. Condensation of this phase near the solidus yields peralkaline phases such as cryolite, and also HFSE minerals, and imparts to the albite-rich granite body a generally strong but variable peralkaline character. Although marked analogies have been noted between the Madeira and the Erzgebirge albite granites, one critical difference concerns the respective development of the peralkaline *versus* peraluminous stages, respectively strongly marked and non-existent at Pitinga, and weakly marked and dominant in the Erzgebirge. This difference can be attributed to the composition of the parental magmas, inferred to be slightly peralkaline to metaluminous at Pitinga and metaluminous to peraluminous in the Erzgebirge (Thomas *et al.* 2006). The composition of the parental magmas will also likely influence the composition and density of the separated peralkaline phase. At Pitinga, the relatively dense peralkaline fluid (as it contains high concentrations of silicates, F, alkalis and HFSE) would favor its preservation relatively deep in the system. Condensation of mineral phases will subsequently generate low-density vapors that may penetrate to shallower levels, react with the apical parts of the albite-rich granite body and produce the autometasomatic processes recorded in the border facies of the albite-rich granite.

## CONCLUSIONS

1. The 1818 Ma Madeira albite-rich granite is a subsolvus magmatic rock that originated by the crystallization of a residual melt, as indicated by its modal composition, mineral chemistry, and whole-rock geochemistry data. The melt was strongly enriched in F, Na, Rb, HFSE, Li, Sn and rare metals. The albite-rich granite is composed of two facies, a dominant, core facies and a border facies, situated along the top and border zones of the albite-rich granite sheet. The core facies is peralkaline and cryolite-bearing, and the border albite-rich granite facies is peraluminous to metaluminous, oxidized, and fluorite-bearing. Mineralogical, petrographic, and geochemical data, as well as the spatial disposition of the border albite-rich granite facies, show that the border albite-rich granite facies is the product of late hydrothermal processes that affected the actual core facies. The consanguinity of the two facies is attested by the transitional contacts between the core and border facies, observed in outcrops, and the similar chemical composition of K-feldspar and albite of both facies. The contact relationships between the core facies and the porphyritic hypersolvus alkali feldspar granite, and the mildly transitional, metaluminous to peralkaline geochemical signature of the latter, indicate that both facies were comagmatic and coeval. The available data demonstrate that the Madeira albite-rich granite, the porphyritic hypersolvus alkali feldspar granite and the nearby peralkaline Europa granite are not comagmatic (the Europa pluton is slightly older, 1829 Ma).

2. The feldspars from the albite-rich granite are near end-members K-feldspar and albite, both containing up to 1 wt% Fe<sub>2</sub>O<sub>3</sub>, and the K-feldspar is Rb-rich. Two types of Li-rich micas were identified in the albite-rich granite: polyolithionite and a lithian annite. The micas are Zn- and Rb-rich, with K/Rb values in the same range as displayed by evolved, fractionated pegmatites. The cassiterite crystals are zoned, with a Nb-, Ta-, and Fe-rich core and an almost end-member SnO<sub>2</sub> rim, indicating a magmatic origin. The magnetite crystals are also near the end member in composition, showing very low Ti contents and no ilmenite exsolution-induced lamellae, constraining magnetite crystallization (and that of the albite-rich granite) below 600°C (Burton 1991).

3. The core albite-rich granite was derived from a highly fractionated, low-viscosity, fluorine-rich, H<sub>2</sub>O-bearing melt. The crystallization of this liquid started at a low temperature, probably at or below 700°C, with quartz as the liquidus phase owing to the influence of the high F contents (Manning 1981, Kovalenko & Kovalenko 1984). The crystallizing melt reached the Qtz – K-feldspar cotectic at around 650°C (Xiong *et al.* 1999). Upon decreasing temperature, the ternary feldspar solvus was reached, and albite crystallized together with quartz and K-feldspar down to

the solidus. Because of the high concentrations of F, the solidus was strongly depressed, further extending the crystallization interval and allowing continuous re-equilibration of feldspar compositions along the solvus. At the solidus (around 500°C), the feldspars approach end-member compositions.

4. The mineralogical and geochemical aspects suggest that the parental melt of the Madeira albite-rich granite most probably was not originally peralkaline, but rather acquired this character in the course of the differentiation processes established after the emplacement of the albite-rich granite sheet.

5. The F-rich peralkaline melt that produced the albite-rich granite core facies is probably the result of a phase-separation process, or immiscibility, similar to that registered by Thomas *et al.* (2006) in the Erzgebirge. The peralkaline phase had separated from a parental melt, most probably slightly peralkaline to metaluminous, with a composition similar to that of the porphyritic hypersolvus alkali feldspar granite. The high density of this peralkaline phase (in comparison with normal hydrothermal fluids) allowed its preservation deep in the Madeira pluton.

## ACKNOWLEDGEMENTS

The Paranapanema Group gave support for field work and provided access to unpublished data and CNPq gave financial support (HTC: 141927/96–8; RD: 400038/99, 463196/2000–7; 307469/2003–4). OTR acknowledges financial support from the Academy of Finland (SA 30600). The Microprobe Laboratory of Brasília University for microprobe analyses, Prof. Henrique Khan of the LCT at the University of São Paulo for access to SEM, Marc Chausson and Denis Mangin of the CRPG (Vandoeuvre, France) for ion-microprobe analyses and support during analytical work, Bruno Scaillet for discussions about alkaline granites, are gratefully acknowledged. Prof. Milan Rieder is thanked for helpful comments on the mineral chemistry of the micas. The original manuscript benefited from constructive reviews and critical comments by Bernard Bonin and the Editor, Robert F. Martin that contributed to its improvement. This paper is the contribution number 2 to the Brazilian Institute of Amazonia Geosciences (INCT program CNPq/MCT/FAPESPA, 573733/2008-2).

## REFERENCES

- ALMEIDA, F.F.M., BRITO NEVES, B.B. & CARNEIRO, C.D.R. (2000): The origin and evolution of the South American Platform. *Earth-Sci. Rev.* **50**, 77-111.
- ALMEIDA, J.A.C. (2002): *Estudo de suscetibilidade magnética e caracterização dos minerais óxidos de Fe e Ti do Granito Madeira, Pitinga, Amazonas*. Honors Thesis, Centro de Geociências, Universidade Federal do Pará, Belém, Brazil.

- BADANINA, E.V., VEKSLER, I.V., THOMAS, R., SYRITSO, L.F. & TRUMBULL, R.B. (2004): Magmatic evolution of Li-F, rare-metal granites: a case study of melt inclusions in the Khangilay complex, Eastern Transbaikalia (Russia). *Chem. Geol.* **210**, 113-133.
- BAILEY, D.K. & MACDONALD, R. (1970): Petrochemical variations among mildly peralkaline (comendite) obsidians from the oceans and continents. *Contrib. Mineral. Petrol.* **28**, 340-351.
- BAKER, B.H. & MCBIRNEY, A.R. (1985): Liquid fractionation. III. Geochemistry of zoned magmas and the compositional effects of liquid fractionation. *J. Volcanol. Geotherm. Res.* **24**, 55-81.
- BASTOS NETO, A., PEREIRA, V.P., LIMA, E.F., FERRON, J.M.T.M., MINUZZI, O.R.R., PRADO, M., RONCHI, L.H., FLORES, J.A.A., FRANTZ, J.C., PIRES, A.C., PIROSAN, R., HOFF, R., BOTELHO, N.F., ROLIM, S.B., ROCHA, F. & ULMANN, L. (2005): A jazida de criolita da mina Pitinga (Amazonas). In Caracterização de Depósitos Mineraiis em Distritos Mineiros da Amazônia (O.J. Marini, E. Queiroz & B.W. Ramos, eds.). Agência para o Desenvolvimento da Indústria Mineral Brasileira – Departamento Nacional da Produção Mineral (ADIMB/DNPM), 477-552.
- BETTENCOURT, J.S., TOSDAL, R.M., LEITE, W.B., JR. & PAYOLLA, B.L. (1999): Mesoproterozoic rapakivi granites of the Rondônia Tin Province, southwestern border of the Amazonian craton, Brazil. I. Reconnaissance U–Pb geochronology and regional implications. *Precamb. Res.* **95**, 41-67.
- BEUS, A. A. (1982): Metallogeny of Precambrian rare-metal granitoids. *Rev. Bras. Geoc.* **12**, 410-413.
- BONIN, B. (1996): A-type granite ring complexes: mantle origin through crustal filters and the anorthosite–rapakivi magmatism connection. In Petrology and Geochemistry of Magmatic Suites of Rocks in the Continental and Oceanic Crusts (D. Demaiffe, ed.). Université Libre de Bruxelles – Musée Royal de l’Afrique Centrale, Bruxelles, Belgique (201-217).
- BORGES, R.M.K., DALL’AGNOL, R. & COSTI, H.T. (2003): Geologia, petrografia e química mineral das micas dos greisens estaníferos associados ao pluton Água Boa, Pitinga (AM). *Rev. Bras. Geoc.* **33**, 51-62.
- BORGES, R.M.K., VILLAS, R.N.N., FUZIKAWA, K., DALL’AGNOL, R. & PIMENTA, M.A. (2009): Phase separation, fluid mixing, and origin of the greisens and potassic episyenite associated with the Água Boa pluton, Pitinga tin province, Amazonian Craton, Brazil. *J. S. Am. Earth. Sci.* **27**, 161-183.
- BOWDEN, P. & KINNAIRD, J.A. (1984): Geology and mineralization of the Nigerian anorogenic ring complexes. *Geol. Jahrb.* **B56**, 1-65.
- BRITO NEVES, B.B. & CORDANI, U.G. (1991): Tectonic evolution of South America during the Late Proterozoic. *Precamb. Res.* **53**, 23-40.
- BURTON, B.P. (1991): The interplay of chemical and magnetic ordering. In Oxide Minerals: Petrologic and Magnetic Significance (D.H. Lindsley, ed.). *Rev. Mineral.* **25**, 303-322.
- CARMICHAEL, I.S.E. (1967): The mineralogy and petrology of the volcanic rocks from Leucite Hills, Wyoming. *Contrib. Mineral. Petrol.* **15**, 24-66.
- ČERNÝ, P. & BURT, D.M. (1984): Paragenesis, crystallochemical characteristics, and geochemical evolution of micas in granite pegmatites. In Micas (S.W. Bailey, ed.). *Rev. Mineral.* **13**, 257-297.
- ČERNÝ, P., MEINTZER, R.E. & ANDERSON, A.J. (1985a): Extreme fractionation in rare-element granitic pegmatites: selected examples of data and mechanisms. *Can. Mineral.* **23**, 381-421.
- ČERNÝ, P., PENTINGHAUS, H. & MACEK, J.J. (1985b): Rubidian microcline from Red Cross Lake, northeastern Manitoba. *Bull. Geol. Soc. Finland* **57**, 217-230.
- CHAROY, B., CHAUSSIDON, M. & NORONHA, F. (1995): Lithium zonation in white micas from the Argemela microgranite (central Portugal): an in situ ion-, electron-microprobe and spectroscopic investigation. *Eur. J. Mineral.* **7**, 335-352.
- COLLINS, W.J., BEAMS, S.D., WHITE, A.J.R. & CHAPPELL, B.W. (1982): Nature and origin of A-type granites with particular reference to southeastern Australia. *Contrib. Mineral. Petrol.* **80**, 189-200.
- COSTI, H.T. (2000): *Petrologia de granitos alcalinos com alto flúor mineralizados em metais raros: o exemplo do albita-granito da mina Pitinga, Amazonas, Brasil*. Doctorate thesis, Universidade Federal do Pará, Belém, Brazil.
- COSTI, H.T., DALL’AGNOL, R., BORGES, R.M.K., MINUZZI, O.R.R. & TEIXEIRA, J.T. (2002): Tin-bearing sodic episyenites associated with the Proterozoic, A-type Água Boa granite, Pitinga mine, Amazonian craton, Brazil. *Gondwana Res.* **5**, 435-451.
- COSTI, H.T., DALL’AGNOL, R. & MOURA, C.A.V. (2000a): Geology and Pb–Pb geochronology of Paleoproterozoic volcanic and granitic rocks of the Pitinga Province, Amazonian craton, northern Brazil. *Int. Geol. Rev.* **42**, 832-849.
- COSTI, H.T., HORBE, A.M.C., BORGES, R.M.K., DALL’AGNOL, R., ROSSI, A. & SIGHINOLFI, G.P. (2000b): Mineral chemistry of cassiterites from Pitinga Province, Amazonian craton. *Rev. Bras. Geoc.* **30**, 775-782.
- CUNNEY, M., MARGINAC, C. & WEISBROD, A. (1992): The Beauvoir topaz–lepidolite granite (Massif Central, France): the disseminated magmatic Sn–Li–Ta–Nb–Be mineralization. *Econ. Geol.* **87**, 1766-1794.
- CURRIE, K.L. (1997): A revised computer program for amphibole classification. *Can. Mineral.* **35**, 1351-1352.
- DALL’AGNOL, R., COSTI, H.T., LEITE, A.A.S., MAGALHÃES, M.S. & TEIXEIRA, N.P. (1999): Rapakivi granites from Brazil and adjacent areas. *Precamb. Res.* **95**, 9-39.

- DALL'AGNOL, R. & OLIVEIRA, D.C. (2007): Oxidized, magnetite-series, rapakivi-type granites of Carajás, Brazil: implications for classification and petrogenesis of A-type granites. *Lithos* **93**, 215-233.
- DALL'AGNOL, R., TEIXEIRA, N.P. & MAGALHÃES, M.S. (1993): Diagnostic features of the tin-specialized anorogenic granites of the eastern Amazonian region. *An. Acad. Bras. Cienc.* **65**, 33-50.
- DALL'AGNOL, R., TEIXEIRA, N.P., RĂMÔ, O.T., MOURA, C.A.V., MACAMBIRA, M.J.B. & OLIVEIRA, D.C. (2005): Petrogenesis of the Paleoproterozoic rapakivi A-type granites of the Archean Carajás metallogenic province, Brazil. *Lithos* **80**, 101-129.
- DAOUD, W.K. (1988): *Granitos estaníferos de Pitinga, Amazonas: contexto geológico e depósitos minerais associados*. Master's thesis, Universidade de Brasília, Brazil.
- DEER, W.A., HOWIE, R.A. & ZUSSMAN, J. (1963): *Rock-Forming Minerals. 4. Framework Silicates*. Longmans, Green and Co., Ltd., London, U.K.
- DINGWELL, D.B. (1988): The structures and properties of fluorine-rich magmas: a review of experimental studies. In *Recent Advances in the Geology of Granite-Related Mineral Deposits* (R.P. Taylor & D.F. Strong, eds.). *Can. Inst. Mining Metall., Spec. Vol.* **39**, 1-12.
- DINGWELL, D.B., HESS, K.-U. & ROMANO, C. (1998): Extremely fluid behavior of hydrous peralkaline rhyolites. *Earth Planet. Sci. Lett.* **158**, 31-38.
- DOLEJS, D. & BAKER, D.R. (2004): Thermodynamic analysis of the system  $\text{Na}_2\text{O}-\text{K}_2\text{O}-\text{CaO}-\text{Al}_2\text{O}_3-\text{SiO}_2-\text{H}_2\text{O}-\text{F}_2\text{O}^{-1}$ : stability of fluorine-bearing minerals in felsic igneous suites. *Contrib. Mineral. Petrol.* **146**, 762-778.
- DOLEJS, D. & BAKER, D.R. (2007a): Liquidus equilibria in the system  $\text{K}_2\text{O}-\text{Na}_2\text{O}-\text{Al}_2\text{O}_3-\text{SiO}_2-\text{F}_2\text{O}^{-1}-\text{H}_2\text{O}$  to 100 MPa. I. Silicate-fluoride liquid immiscibility in anhydrous systems. *J. Petrol.* **48**, 785-806.
- DOLEJS, D. & BAKER, D.R. (2007b): Liquidus equilibria in the system  $\text{K}_2\text{O}-\text{Na}_2\text{O}-\text{Al}_2\text{O}_3-\text{SiO}_2-\text{F}_2\text{O}^{-1}-\text{H}_2\text{O}$  to 100 MPa. II. Differentiation paths of fluorosilicic magmas in hydrous systems. *J. Petrol.* **48**, 807-828.
- EKWERE, S.J. & OLADE, M.A. (1984): Geochemistry of the tin-niobium-bearing granites of the Liruei (Ririwai) Complex, Younger Granite Province, Nigeria. *Chem. Geol.* **45**, 225-243.
- FERRON, J.M.T.M., BASTOS NETO, A.C., LIMA, E.F., COSTI, H.T., MOURA, C.A.V., PRADO, M., PIEROSAN, R. & GALARZA, M.A. (2006): Geologia e geocronologia Pb-Pb de rochas graníticas e vulcânicas ácidas a intermediárias paleoproterozoicas da Província Pitinga, craton Amazônico. *Rev. Bras. Geoc.* **36**, 499-512.
- FERRON, J.M.T.M., BASTOS NETO, A.C., LIMA, E.F., NARDI, L.V.S., COSTI, H.T., PIEROSAN, R. & PRADO, M. (in press): Petrology, geochemistry, and geochronology of paleoproterozoic volcanic and granitic rocks (1.89 to 1.88 Ga) of the Pitinga Province, Amazonian Craton, Brazil. *J. S. Am. Earth. Sci.*
- FOSTER, M.D. (1960): Interpretation of the composition of lithium micas. *U.S. Geol. Surv., Prof. Pap.* **354-E**, 115-146.
- FROST, C.D., FROST, B.R., BELL, J.M. & CHAMBERLAIN, K.R. (2002): The relationship between A-type granites and residual magmas from anorthosite: evidence from the northern Sherman batholith, Laramie Mountains, Wyoming, USA. *Precamb. Res.* **119**, 45-71.
- GIBBS, A.K. & BARRON, C.N. (1983): The Guiana Shield reviewed. *Episodes* **2**, 7-13.
- GLYUK, D.S. & ANFILOGOV, N.V. (1973). Phase equilibria in the system granite-H<sub>2</sub>O-HF at a pressure of 1000 kg/cm<sup>2</sup>. *Geochem. Int.* **10**, 321-325.
- HAAPALA, I. (1997): Magmatic and postmagmatic processes in tin-mineralized granites: topaz-bearing leucogranite in the Eurajoki rapakivi granite stock, Finland. *J. Petrol.* **38**, 1645-1659.
- HARRIS, N.B.W. (1981): The role of fluorine and chlorine in the petrogenesis of a peralkaline complex from Saudi Arabia. *Chem. Geol.* **31**, 303-310.
- HELBA, H., TRUMBULL, R.B., MORTEANI, G. & KHALIL, S.O. (1997): Geochemical and petrographic studies of Ta mineralization in the Nuweibi albite granite complex, eastern Desert, Egypt. *Mineral. Deposita* **32**, 164-179.
- HORBE, M.A., HORBE, A.M.C., COSTI, H.T. & TEIXEIRA, J.T. (1991): Geochemical characteristics of cryolite-tin-bearing granites from the Pitinga mine, northwestern Brazil: a review. *J. Geochem. Explor.* **40**, 227-249.
- HUANG, X.L., WANG, R.C., CHEN, X.M., HU, H. & LIU, C.S. (2002): Vertical variations in the mineralogy of the Yichun topaz-lepidolite granite, Jiangxi Province, Southern China. *Can. Mineral.* **40**, 1047-1068.
- JOHANNES, W. & HOLTZ, F. (1996): *Petrogenesis and Experimental Petrology of Granitic Rocks*. Springer-Verlag, Berlin, Germany.
- KEPLER, H. (1993): Influence of fluorine on the enrichment of high field strength trace elements in granitic rocks. *Contrib. Mineral. Petrol.* **114**, 479-488.
- KINNAIRD, J.A., BOWDEN, P., IXER, R.A. & ODLING, N.W.A. (1985): Mineralogy, geochemistry and mineralization of the Ririwai Complex, northern Nigeria. *J. Afr. Earth Sci.* **3**, 185-222.
- KOVALENKO, V.I. (1978): The genesis of rare metal granitoids and related ore deposits. In *Metallization Associated with Acid Magmatism* **3** (M. Štemprok, L. Burnol & G. Tischendorf, eds.). Geological Survey of Czechoslovakia, Prague, Czechoslovakia (235-247).

- KOVALENKO, V.I. & KOVALENKO, N.I. (1984): Problems of the origin, ore-bearing and evolution of rare-metal granitoids. *Phys. Earth Planet. Int.* **35**, 51-62.
- KRETZ, R. (1983): Symbols for rock-forming minerals. *Am. Mineral.* **68**, 277-279
- KUEHNER, S.M. & JOSWIAK, D.J. (1996): Naturally occurring ferric iron sanidine from Leucite Hills lamproite. *Am. Mineral.* **81**, 229-237.
- LAGACHE, M. & QUÉMÉNEUR, J. (1997): The Volta Grande pegmatites, Minas Gerais, Brazil: an example of rare-element granitic pegmatites exceptionally enriched in lithium and rubidium. *Can. Mineral.* **35**, 153-165.
- LEAKE, B.E., WOOLLEY, A.R., ARPS, C.E.S., BIRCH, W.D., GILBERT, M.C., GRICE, J.D., HAWTHORNE, F.C., KATO, A., KISCH, H.J., KRIVOVICHEV, V.G., LINTHOUT, K., LAIRD, J., MANDARINO, J.A., MARESCH, W.V., NICKEL, E.H., ROCK, N.M.S., SCHUMACHER, J.C., SMITH, D.C., STEPHENSON, N.C.N., UNGARETTI, L., WHITTAKER, E.J.W. & GUO, YOUZHI (1997): Nomenclature of amphiboles: report of the Subcommittee on Amphiboles of the International Mineralogical Association, Commission on New Minerals and Mineral Names. *Eur. J. Mineral.* **9**, 623-651.
- LEITE, W.B., JR. (2002): *A Suíte Intrusiva Santa Clara (RO) e a mineralização primária polimetálica (Sn, W, Nb, Ta, Zn, Cu e Pb) associada*. Doctorate thesis, Instituto de Geociências, Universidade de São Paulo, São Paulo, Brazil.
- LENHARO, S.L.R., MOURA, M.A. & BOTELHO, N.F. (2002): Petrogenetic and mineralization processes in Paleo- to Mesoproterozoic rapakivi granites: examples from Pitinga and Goiás, Brazil. *Precamb. Res.* **119**, 277-299.
- LENHARO, S.L.R., POLLARD, P.J. & BORN, H. (2003): Petrology and textural evolution of granites associated with tin and rare-metals mineralization at the Pitinga mine, Amazonas, Brazil. *Lithos* **66**, 37-61.
- LINNEN, R.L. (1998): The solubility of Nb-Ta-Zr-Hf-W in granitic melts with Li and Li+F: constraints for mineralization in rare metal granites and pegmatites. *Econ. Geol.* **93**, 1013-1025.
- LINNEN, R.L., PICHAVANT, M. & HOLTZ, F. (1996): The combined effects of  $fO_2$  and melt composition on  $SnO_2$  solubility and tin diffusivity in haplogranitic melts. *Geochim. Cosmochim. Acta* **60**, 4965-4976.
- LINTHOUT, K. & LUSTENHOUWER, W.J. (1993): Ferrian high sanidine in a lamproite from Cancarix, Spain. *Mineral. Mag.* **57**, 289-299.
- LONDON, D. (1992): The application of experimental petrology to the genesis and crystallization of granitic pegmatites. *Can. Mineral.* **30**, 499-540.
- LONDON, D., MORGAN, G.B., VI & HERVIG, R.L. (1989): Vapor-undersaturated experiments with Macusani glass +  $H_2O$  at 200 MPa, and the internal differentiation of granitic pegmatites. *Contrib. Mineral. Petrol.* **102**, 1-17.
- LUKKARI, S. & HOLTZ, F. (2007): Phase relations of a F-enriched peraluminous granite: an experimental study of the Kymi topaz granite stock, southern Finland. *Contrib. Mineral. Petrol.* **153**, 273-288.
- MACAMBIRA, M.J.B., TEIXEIRA, J.T., DAOUD, W.K. & COSTI, H.T. (1987): Geochemistry, mineralization and age of tin-bearing granites from Pitinga, northwestern Brazil. *Rev. Bras. Geoc.* **17**, 562-570.
- MACDONALD, R., DAVIES, G.R., BLISS, C.M., LEAT, P.T., BAILEY, D.K. & SMITH, R.L. (1987): Geochemistry of high-silica peralkaline rhyolites, Naivasha, Kenia Rift Valley. *J. Petrol.* **28**, 979-1008.
- MANNING, D.A.C. (1981): The effect of fluorine on liquidus phase relationships in the system Qz-Ab-Or with excess water at 1 kb. *Contrib. Mineral. Petrol.* **76**, 206-215.
- MANNING, D.A.C. & PICHAVANT, M. (1988): Volatiles and their bearing on the behaviour of metals in granitic systems. In *Recent Advances in the Geology of Granite-Related Mineral Deposits* (R.P Taylor & D.F. Strong, eds.). *Can. Inst. Mining. Metall., Spec. Vol.* **39**, 13-24.
- MARTIN, R.F. (2006): A-type granites of crustal origin ultimately result from open-system fenitization-type reactions in an extensional environment. *Lithos* **91**, 125-136.
- MINUZZI, O.R.R. (2005): *Gênese e evolução da mineralização de criolita, pirocloro e columbita da subfácies albita granito de núcleo, mina Pitinga, Amazonas, Brasil*. Doctorate thesis, Universidade Federal do Rio Grande do Sul, Porto Alegre, Brazil.
- MINUZZI, O.R.R., BASTOS NETO, A.C., FORMOSO, M.L.L., ANDRADE, S., JANASI, V.A. & FLORES, J.A.A. (2008): Rare earth element and yttrium geochemistry applied to the genetic study of cryolite ore at the Pitinga mine (Amazon, Brazil). *An. Acad. Bras. Cienc.* **80**, 719-733.
- MÖLLER, P., DULSKI, P., SZACKI, W., MALOW, G. & RIEDEL, E. (1988): Substitution of tin in cassiterite by tantalum, niobium, tungsten, iron and manganese. *Geochim. Cosmochim. Acta* **52**, 1497-1503.
- MONIER, G. & ROBERT, J.-L. (1986): Evolution of the miscibility gap between muscovite and biotite solid solutions with increasing lithium content: an experimental study in the system  $K_2O-Li_2O-MgO-FeO-Al_2O_3-SiO_2-H_2O-HF$  at 600°C, 2 kbar  $P_{H_2O}$ : comparison with natural lithium micas. *Mineral. Mag.* **50**, 641-651.
- NARDI, L.V.S. & BONIN, B. (1991): Post-orogenic and non-orogenic alkaline granite associations: the Saibro intrusive suite, southern Brazil – a case study. *Chem. Geol.* **92**, 197-211.
- NEIVA, A.M.R. (1996): Geochemistry of cassiterite and its inclusions and exsolution products from tin and tungsten deposits in Portugal. *Can. Mineral.* **34**, 745-768.
- PICHAVANT, M. (1997): Genesis of granite-related mineralization: the importance of magmatic processes. In *Second*

- Int. Symp. Granites and Associated Mineralizations (Salvador), Extended Abstr. and Program (V.P. Ferreira & A.N. Sial, eds.). SGM (78-79).
- PICHAVENT, M., BOHER, M., STENGER, J.-F., AISSA, M. & CHAROY, B. (1987): Relations de phase des granites de Beauvoir à 1 et 3 kbar, en conditions de saturation en H<sub>2</sub>O. *Géol. France* **2**, 77-86.
- PICHAVENT, M. & MANNING, D.A.C. (1984): Petrogenesis of tourmaline granites and topaz granites: the contribution of experimental data. *Phys. Earth Planet. Int.* **35**, 31-50.
- POLLARD, P.J. (1995): A special issue devoted to the geology of rare metal deposits: an introduction and overview. *Econ. Geol.* **90**, 489-494.
- PRESTON, R.F., STEVENS, G. & MCCARTHY, T.S. (2003): Fluid compositions in equilibrium with silica-undersaturated magmas in the system Na<sub>2</sub>O-Al<sub>2</sub>O<sub>3</sub>-SiO<sub>2</sub>-H<sub>2</sub>O: clues to the composition of fenitizing fluids. *Contrib. Mineral. Petrol.* **144**, 559-569.
- RÄMÖ, O.T. (1991): Petrogenesis of the Proterozoic rapakivi granites and related basic rocks of the southeastern Fennoscandian: Nd and Pb isotopic and general geochemical constraints. *Geol. Surv. Finland Bull.* **355**.
- RIEDER, M., CAVAZZINI, G., D'YAKONOV, Y., FRANK-KAMENETSKII, V.A., GOTTARDI, G., GUGGENHEIM, S., KOVAL, P.V., MÜLLER, G., NEIVA, A.M.R., RADOSLOVICH, E.W., ROBERT, J.-L., SASSI, F.P., TAKEDA, H., WEISS, Z. & WONES, D.R. (1998): Nomenclature of the micas. *Clays Clay Mineral.* **46**, 586-595.
- SADOWSKI, G.R. & BETTENCOURT, J.S. (1996): Mesoproterozoic tectonic correlations between eastern Laurentia and the western border of the Amazon craton. *Precamb. Res.* **76**, 213-227.
- SANTOS, J.O.S., HARTMANN, L.A., GAUDETTE, H.E., GROVES, D.L., MCNAUGHTON, N.J. & FLETCHER, I.R. (2000): A new understanding of the provinces of the Amazon craton based on integration of field mapping and U-Pb and Sm-Nd geochronology. *Gondwana Res.* **3**, 453-488.
- SANTOS, J.O.S., HARTMANN, L.A., MCNAUGHTON, N.J. & FLETCHER, I.R. (2002): Timing of mafic magmatism in the Tapajós Province (Brazil) and implications for the evolution of the Amazon craton. *J. S. Am. Earth Sci.* **15**, 409-429.
- SCAILLET, B. & MACDONALD, R. (2001): Phase relations of peralkaline silicic magmas and petrogenetic implications. *J. Petrol.* **42**, 825-845.
- SCAILLET, B. & MACDONALD, R. (2003): Experimental constraints on the relationships between peralkaline rhyolites of the Kenya Rift Valley. *J. Petrol.* **44**, 1867-1894.
- SCHWARTZ, M.O. (1992): Geochemical criteria for distinguishing magmatic and metasomatic albite-enrichment in granitoids – examples from the Ta-Li granite Yichun (China) and the Sn-W deposit Tikus (Indonesia). *Mineral. Deposita* **27**, 101-108.
- SMITH, J.V. & BROWN, W.L. (1988): *Feldspar Minerals. 1. Crystal Structures, Physical, Chemical and Microtextural Properties* (2<sup>nd</sup> ed.). Springer-Verlag, Berlin, Germany.
- SPEAR, F.S. (1993): *Metamorphic Phase Equilibria and Pressure – Temperature – Time Paths*. Mineralogical Society of America, Washington, D.C.
- ŠTEMPROK, M. & ŠULCEK, Z. (1969): Geochemical profile through an ore-bearing lithium granite. *Econ. Geol.* **64**, 392-404.
- SUN, S. & YU, J. (1999): Fe-Li micas: a new approach to the substitution series. *Miner. Mag.* **63**, 933-945.
- TASSINARI, C.C.G. & MACAMBIRA, M.J.B. (1999): Geochronological provinces of the Amazonian craton. *Episodes* **22**, 174-182.
- TAYLOR, R.P. (1992): Petrological and geochemical characteristics of the Pleasant Ridge zinnwaldite-topaz granite, southern New Brunswick, and comparisons with other topaz-bearing felsic rocks. *Can. Mineral.* **30**, 895-921.
- TEIXEIRA, N.P., BETTENCOURT, J.S., MOURA, C.A.V., DALL'AGNOL, R. & MACAMBIRA, E.M.B. (2002): Archean crustal sources for Paleoproterozoic tin-mineralized granites in the Carajás Province, SSE Pará, Brazil: Pb-Pb geochronology and Nd isotope geochemistry. *Precamb. Res.* **119**, 257-275.
- THOMAS, R., FÖRSTER, H.-J., RICKERS, K. & WEBSTER, J.D. (2005): Formation of extremely F-rich hydrous melt fractions and hydrothermal fluids during differentiation of highly evolved tin-granite magmas: a melt/fluid-inclusion study. *Contrib. Mineral. Petrol.* **148**, 582-601.
- THOMAS, R., WEBSTER, J.D., RHEDE, D., SEIFERT, W., RICKERS, K., FÖRSTER, H.-J., HEINRICH, W. & DAVIDSON, P. (2006): The transition from peraluminous to peralkaline granitic melts: evidence from melt inclusions and accessory minerals. *Lithos* **91**, 137-149.
- TINDLE, A.G. & WEBB, P.C. (1990): Estimation of lithium contents in trioctahedral micas using microprobe data: application to micas from granitic rocks. *Eur. J. Mineral.* **2**, 595-610.
- TUTTLE, O.F. & BOWEN, N.L. (1958): Origin of granite in the light of experimental studies in the system NaAlSi<sub>3</sub>O<sub>8</sub>-KAlSi<sub>3</sub>O<sub>8</sub>-SiO<sub>2</sub>-H<sub>2</sub>O. *Geol. Soc. Am., Mem.* **74**.
- VEIGA, J.P., JR., NUNES, A.C.B., FERNANDES, A.S., AMARAL, J.A.F., AMARAL, J.E., PESSOA, M.R. & CRUZ, S.A.S. (1979): *Projeto Sulfetos de Uatumã*. Departamento Nacional da Produção Mineral – Companhia de Pesquisa de Recursos Minerais (DNP/CPRM), Manaus, Brazil (in 7 vol.).

- VEKSLER, I.V. & THOMAS, R. (2002): An experimental study of B-, P- and F-rich synthetic granite pegmatite at 0.1 and 0.2 GPa. *Contrib. Mineral. Petrol.* **143**, 673-683.
- VEKSLER, I.V., THOMAS, R. & SCHMIDT, C. (2002): Experimental evidence of three coexisting immiscible fluids in synthetic granitic pegmatite. *Am. Mineral.* **87**, 775-779.
- WEBSTER, J.D. (1990): Partitioning of F between H<sub>2</sub>O and CO<sub>2</sub> fluids and topaz rhyolite melt. Implications for mineralizing magmatic-hydrothermal fluids in F-rich granitic systems. *Contrib. Mineral. Petrol.* **104**, 424-438.
- WEBSTER, J.D. & REBBERT, C.R. (1998): Experimental investigation of H<sub>2</sub>O and Cl<sup>-</sup> solubilities in F-enriched silicate liquids; implications for volatile saturation of topaz rhyolite magmas. *Contrib. Mineral. Petrol.* **132**, 198-207.
- WEBSTER, J.D., THOMAS, R., FÖRSTER, H.-J., SELTMANN, R. & TAPPEN, C. (2004): Geochemical evolution of halogen-enriched granite magmas and mineralizing fluids of the Zinnwald tin-tungsten mining district, Erzgebirge, Germany. *Mineral. Deposita* **39**, 452-472.
- WEIDNER, J.R. & MARTIN, R.F. (1987): Phase equilibria of a fluorine-rich leucogranite from the St. Austell pluton, Cornwall. *Geochim. Cosmochim. Acta* **51**, 1591-1597.
- WHALEN, J.B., CURRIE, K.L. & CHAPPELL, B.W. (1987): A-type granites: geochemical characteristics, discrimination and petrogenesis. *Contrib. Mineral. Petrol.* **95**, 407-419.
- WYLLIE, P.J. & TUTTLE, O.F. (1961): Experimental investigation of silicate systems containing two volatile components. II. The effects of NH<sub>3</sub> and HF, in addition to H<sub>2</sub>O, on the melting temperatures of albite and granite. *Am. J. Sci.* **259**, 128-143.
- XIONG, X.L., RAO, B., CHEN, F.R., ZHU, J.C. & ZHAO, Z.H. (2002): Crystallization and melting experiments of a fluorine-rich leucogranite from the Xianghualing Pluton, South China, at 150 MPa and H<sub>2</sub>O-saturated conditions. *J. Asian Earth Sci.* **21**, 175-188.
- XIONG, X.L., ZHAO, Z.H., ZHU, J.C. & RAO, B. (1999): Phase relations in albite granite-H<sub>2</sub>O-HF system and their petrogenetic applications. *Geochem. J.* **33**, 199-214.
- YIN, L., POLLARD, P.J., SHOUXI, H. & TAYLOR, R.G. (1995): Geologic and geochemical characteristics of the Yichun Ta-Nb-Li deposit, Jiangxi Province, South China. *Econ. Geol.* **90**, 577-585.

Received November 20, 2007, revised manuscript accepted September 17, 2009

